AD-A175 561 EFFECT OF DYNAMIC STALL AND ELASTIC PARAMETERS ON THE FUNDAMENTAL MECHANI..(U) GEORGIA INST OF TECH ATLANTA SCHOOL OF AEROSPACE ENGINEERING.. D A PETERS 01 NOV 86 1/1

UNCLASSIFIED ARO023322.7-EG DAAG29-85-K-0228 F/G 1/3 NL

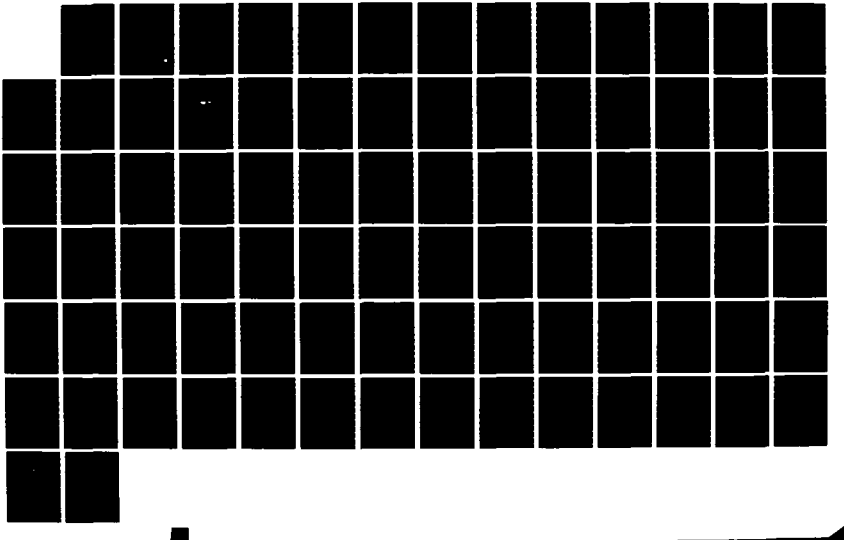

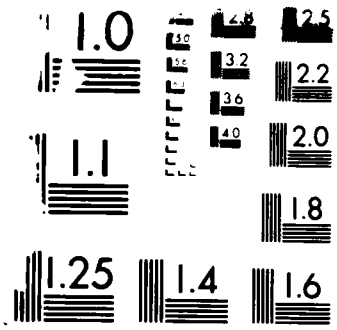
1.0
1.1
1.25
1.4
1.6
1.8
2.0
2.2
2.5
3.2
3.6
4.0

FINAL REPORT

EFFECT OF DYNAMIC STALL AND ELASTIC PARAMETERS ON THE FUNDAMENTAL MECHANISMS OF HELICOPTER VIBRATIONS

David A. Peters

Prepared for

U.S. Army Research Office
P.O. Box 12211
Research Triangle Park, NC 27709-2211

Under

Contract No. DAAG29-85-K-0228

November 1986

GEORGIA INSTITUTE OF TECHNOLOGY
A UNIT OF THE UNIVERSITY SYSTEM OF GEORGIA
SCHOOL OF AEROSPACE ENGINEERING
ATLANTA, GEORGIA 30332

1986

UNCLASSIFIED

SECURITY CLASSIFICATION OF THIS PAGE *(When Data Entered)*

REPORT DOCUMENTATION PAGE		READ INSTRUCTIONS BEFORE COMPLETING FORM
1. REPORT NUMBER ARO 23322.7-EG	2. GOVT ACCESSION NO. NA	3. RECIPIENT'S CATALOG NUMBER NA
4. TITLE *(and Subtitle)* Effect of Dynamic Stall and Elastic Parameters on the Fundamental Mechanisms of Helicopter Vibrations		5. TYPE OF REPORT & PERIOD COVERED Final Report Sept. 1, 1985 to Sept.30,1986 6. PERFORMING ORG. REPORT NUMBER
7. AUTHOR(s) David A. Peters		8. CONTRACT OR GRANT NUMBER(s) DAAG29-85-K-0228
9. PERFORMING ORGANIZATION NAME AND ADDRESS School of Aerospace Engineering Georgia Institute of Technology Atlanta, Georgia 30332		10. PROGRAM ELEMENT, PROJECT, TASK AREA & WORK UNIT NUMBERS NA
11. CONTROLLING OFFICE NAME AND ADDRESS U. S. Army Research Office P. O. Box 12211 Research Triangle Park, NC 27709-2211		12. REPORT DATE Nov. 1, 1986 13. NUMBER OF PAGES
14. MONITORING AGENCY NAME & ADDRESS*(if different from Controlling Office)*		15. SECURITY CLASS. *(of this report)* UNCLASSIFIED 15a. DECLASSIFICATION/DOWNGRADING SCHEDULE

16. DISTRIBUTION STATEMENT *(of this Report)*

Approved for public release; distribution unlimited.

17. DISTRIBUTION STATEMENT *(of the abstract entered in Block 20, if different from Report)*

NA

18. SUPPLEMENTARY NOTES

The view, opinions and/or findings contained in this report are those of the author(s) and should not be construed as an official Department of the Army position, policy, or decision, unless so designated by other documentation.

19. KEY WORDS *(Continue on reverse side if necessary and identify by block number)*

Helicopter, Vibration, Stall

20. ABSTRACT *(Continue on reverse side if necessary and identify by block number)*

This research has dealt with the modeling and solution of rotary-wing dynamics. In the modeling area, it deals with elastic-blade models, ways to introduce rotor-body coupling, aerodynamic behavior near blade-tips, and the modeling of dynamic stall. In solution strategies, we have concentrated on new and improved Floquet methods, on innovative trim methodologies (such as auto-pilot and periodic shooting), on efficient formulation of equations, and on lifting-line and lifting-surface meshes. We have awarded 1 Master of Science and 1 Doctor of Philosophy degree to persons working on the project.

DD FORM 1 JAN 73 1473 EDITION OF 1 NOV 65 IS OBSOLETE

UNCLASSIFIED

SECURITY CLASSIFICATION OF THIS PAGE *(When Data Entered)*

20. ABSTRACT CONTINUED

EFFECT OF DYNAMIC STALL AND ELASTIC PARAMETERS ON THE FUNDAMENTAL MECHANISMS OF HELICOPTER VIBRATIONS

Final Technical Report

by

David A. Peters
Principal Investigator

1 November 1986

U.S. Army Research Office
Grant No: DAAG-29-83-K-0133

Georgia Institute of Technology
School of Aerospace Engineering
Atlanta, GA 30332

Approved for Public Release

Distribution Unlimited

A-1

Table of Contents

1. Introduction

This final report covers 1 year of ARO-sponsored research into the fundamental behavior of rotor dynamics. The original proposal was for 3 years, but the first two years were done under a separate grant. Thus, this report covers only a portion of the originally-proposed work. In this final report, we will summarize the work done, including publications and scientific personnel; and we will provide pertinent technical descriptions of each major area we have pursued.

The philosophy of our research has been to increase the fundamental understanding of those dynamic and aerodynamic phenomena associated with the helicopter. Our approach has been to follow three intertwining lines of research. The first of these is the line of mathematical modeling. Here, we wish both to synthesize and refine mathematical models for various, isolated rotorcraft phenomena, and to learn to couple them together in a systematic way. This is the building-block approach we have followed. The second line of inquiry has been in the development of solution methodologies for these equations. Here, certain solution strategies work better for certain models; and some modeling techniques require new solution strategies. We look specifically at methods that magnify our insight, are computationally efficient, and that can be extended to large-scale systems.

This leads, then, to the third thread of research: basic physical insight. Of course, because we deal with isolated components or with simplified couplings, we do not intend to be able to make predictions on helicopter stability and response that would be applicable to detailed design studies. On the other hand, we do expect our methods to be predictive of the behavior of simplified research models, such as those used by the Army Research and Technology Laboratories. Furthermore, we believe our results give qualitative insight into the physical phenomena present in production rotors. Thus, we try to involve all three elements in our research effort.

2. Statement of Problem

The objectives and scope of this work are as follows:

1) To discover the basic relationships between blade structural parameters and the flap-lag-torsion airloads that result.

2) To determine the extent to which rotor-body coupling affects inplane loads and overall helicopter vibrations.

3) To develop our basic trim procedures to the point at which they can be applied to large, state-of-the-art rotor response program.

4) To determine the effect of dynamic stall on the rotor airloads and on the basic trimming methods.

5) To investigate other methods of obtaining time histories of rotor response, including Hamilton's Law of Varying Action.

Before proceeding to the details of each objective, it is informative to outline the scope in each task. With the exception of item 3, the above objectives are not aimed at the quantitative prediction of helicopter response. They are aimed at obtaining fundamental insight into how rotor vibrations develop and into how they can be efficiently calculated. Thus, in item 1 we consider a simple elastic-blade model with elastic flap, lag, and torsion. Although other, more sophisticated flap-lag-torsion models certainly exist, they have not been obtained under the same assumptions nor with the same purpose in mind as ours. Thus, we have proceeded slowly and carefully to make sure we understand the physical processes at each step.

In item 2, we are looking at a fuselage with 5 rigid body modes and 4 elastic modes (as in our prior work) but with a more detailed rotor model. Naturally, a true fuselage will have many more elastic modes; but we look at a generic frequency sweep that could be representative of several potential modes. Since we have already found that flapping motions drive inplane motions (while inplane effects flapping much less) we make several simplifying assumptions to increase the productivity (and physical interpretations) of the work.

Item 3 is the only area in which we approach the area of applications. These trim procedures are now fairly well understood in terms of theory, and the advancements now come through more sophisticated applications. Therefore, we have reformulated the trim procedures.

Item 4 is a new area of research that developed out of our dynamic-stall work. It is not in our scope to develop any dramatically new dynamic stall procedures. We merely take existing methodologies, investigate how they should be modified to be useful for simplified vibration analyses, and study the resultant effects on the types of calculations we are making.

Item 5 is also a new area of research which developed out of our prior trim investigations. For nearly linear systems, the trim method of periodic shooting is equivalent to finding and inverting the Floquet transition matrix. (An earlier solution method in our research also relied on Floquet theory for vibration analysis.) Thus, it is natural to look for more efficient means of finding the transition matrix. One possibility is the use of Hamilton's Law of Varying Action with comparison functions in time. In this research we study Hamilton's Law in detail with respect to convergence and efficiency.

3. Scientific Personnel and Degrees

Below is a tabulation of those who worked on this project during the past two years along with the degree they have pursued.

Personnel	Man-Months Effort	Degree Sought
David A. Peters	2.2	
Huang Ming-Sheng	4.3	Ph.D
Danny Chiu	4.3	Ph.D
Amir Izadpanah	4.0	Ph.D.*
Robert Longabaugh	4.0	M.S.
Mnaouar Chouchane	-	M.S.**
Cheng-Jian He	2.0	Ph.D.

* Awarded by Georgia Institute of Technology, Sept. 1986

**Awarded by Washington University, Aug. 1986

4. Publications and Reports

1. Karunamoorthy, Swami and Peters, David, "Use of Hierarchical Elastic Blade Equations and Automatic Trim for Helicopter Vibration Analysis", presented at the 42nd Annual National Forum of the American Helicopter Society, Washington, D.C., June 2-4, 1986, Vertica, special issue, 1986.

2. Gaonkar and Peters, "Effectiveness of Current Dynamic Inflow Models in Hover and Forward Flight", Journal of the American Helicopter Society, Vol. 31, No. 2, April 1986.

3. Gaonkar and Peters, "Review of Dynamic Inflow Modeling for Rotorcraft Flight Dynamics", presented at the AIAA 27th SDM meeting, San Antonio, Texas, May 1986.

4. Peters and Chouchane, "Effect of Dynamic Stall on Helicopter Trim and Flap-Lag Response", Fluids and Structures, Vol. I, No. 1, 1986.

5. Izadpanah, Amir, p-Version Finite Elements for the Space-Time Domain with Application to Floquet Theory, Ph.D. Dissertation, Georgia Institute of Technology, Sept. 1986.

6. Chouchane, Mnaouar, Effect of Dynamic Stall on Helicopter Trim and Flap-Lag Response, Master of Science Thesis, Washington University, August 1986.

7. Peters, David and Izadpanah, Amir, "hp-Finite Elements for the Space-Time Domain with Proof of Convergence", presented at the First World Congress on Computational Mechanics, Austin, Texas, Sept. 22-25, 1986, submitted to Computational Mechanics.

8. Huang, Ming-Sheng and Peters, David, "Coupled Elastic Rotor/Body Vibrations with Inplane Degrees of Freedom", ARO workshop on Dynamics and Aeroelastic Modeling of Rotor Systems, Georgia Tech, December 4-5, 1985.

5. Summary of Results

In this section, we summarize the results of our research for this one-year effort. However, (the first two years were performed at Washington University in St. Louis), we will also refer to how this third year completes the work begun in the first two years. Reference numbers refer to publication in Section 4.

5.1 Finite Elements in Time

Recently, much attention has been give to numerical application of Hamilton's Law of varying action. Hamilton's Law is a variational statement about "action" which provides, for the time domain, what variation of work provides in the space domain. Thus, these applications of Hamilton's Law result in finite elements over the time domain; and these can be either p-version, h-version, or a combination of the two (depending on the choice of test functions). However, numerical applications of Hamilton's Law have sometime resulted in solutions that do not converge as the number of elements (i.e., polynomials) is increased. In this research, a convergence proof was found, based on the bilinear formulation, which demonstrates that some formulations are not truly bilinear and may not converge. The proof also leads to an alternate, bilinear formulation of Hamilton's Law for which convergence is assured. The bilinear formulation also leads to an alternative statement about dynamics. In particular, the "virtual action" plus the variation of action over a space-domain must always sum to zero.

Numerical application of the correct bilinear formulation leads to Lagrange multiplier with the physical connotation of an end momentum (which is the analogy of end force in spatial problems). Thus, initial velocity is treated as a "natural" rather than as "geometric" boundary condition; and the Lagrange multiplier converges to the unknown momentum (i.e., velocity) at the end of the time period. Thus, the bilinear formulation is a "mixed method". Accuracies of solutions with the Lagrange multiplier are an order of magnitude better than those which use the derivative of shape functions for velocity.

In the limit as one takes many elements with only a few polynomials each, this formulation reduces to a classical time-marching method, (an h-version finite element) similar to Euler, Runge-Kutta, or predictor correctors. In the limit as many polynomials are used per element, but with only a few elements, the method becomes similar to a Ritz-Galerkin procedure in time (a p-version finite element). Results show that, for any given problem (as characterized by the computational cost of a function evaluation), there is an optimum choice of polynomial number in order to meet any error criterion with minimum computational effort. Similarly, depending on the problem, a particular choice of polynomial number may or may not be more efficient than conventional time-marching methods. In general, finite elements in time become more efficient than marching as the desired accuracy becomes exacting and as function evaluations become computationally expensive.

The details of this work can be found in References 5 and 7. Figures 1-5, taken from Reference 5, summarize the major conclusions of the work. Figure 1 shows the blade flapping angle, β, at the end of one rotor revolution as calculated both by Hamilton's Finite Elements and by our new, bilinear formulation. One can see that, for Hamilton's Law, β fails to converge uniformly as the number of basis functions is increased. Figure 2 further shows that this divergence is not restricted to a certain advance ratio. Results with Hamilton's Law can be in error over 100% even with 12 basis functions at $\mu = 0.5$. The new formulation, on the other hand, converges in all cases.

Figure 3 provides hp-optimization information. The figure gives $\log_{10}$ of the error as a function of the number of floating-point multiplications required in the computation, M. The straight-lines are for various number of polynomials per element, n, with the step size being a running parameter along the lines. One can see that, for any given error tolerance, there is a minimum M given by the interior of optimum curve formed by the locus of straight lines. The x's are results from Hammings predictor-corrector. For this case (C=16 implies 3 to 4 sine or cosine functions in each coefficient), the hp finite elements are always superior to conventional time marching.

Another interesting result of our research can be seen in plots, like Figure 4, which show error on the interior of a large, p-version element. The error norm is zero at t=0 (due to known initial values). It goes through some erratic oscillations (due to truncation errors near x=0), but settles down over the rest of the element. The <u>minimum</u> error, however, is found at $t=\tau$, the end of the period. The values at the end of the period are exactly what is needed for Floquet theory. Thus, finite elements in time (when correctly formulated) are ideal for Floquet applications.

Finally, we consider numerical stability when finite elements are used to march indefinitely, Figure 5. The values ρ and σ are the system frequency and damping multiplied by the element length, Δt. The exterior of the large semi-circles (as well as the interior of the small semi-circles on the ρ axis) are conditions of numerical instability. "n" is the number of polynomials per element. To put this in perspective, typical radii of convergence for other methods are near $2 = 1.4$, smaller than even the n=2 result. At $n = 6$, a step size equal to two periods ($r=3\pi$) is required before instability occurs. From Figure 3, however, we see that such a large step size would result in very large errors with or without the instability. No optimal point on Figure 3 is unstable.

5.2 Dynamic Stall

A major portion of our research has dealt with the introduction of a modified ONERA model (for dynamic stall) into rotor elastic-blade analysis. In this research, reported in References 4 and 6, flap and inplane bending are described by two nonlinear, partial-differential equations which are coupled together as derived in Reference 1. Each equation consists of lower and higher order terms. Approximate solution methods are applied to these aeroelastic equations. The aerodynamic circulations are expressed by our unified theory. Only lower order terms of the equations in Ref. 1 are considered in the analyses. This allows the investigation of the general trends of the result without going into cumbersome computation with little

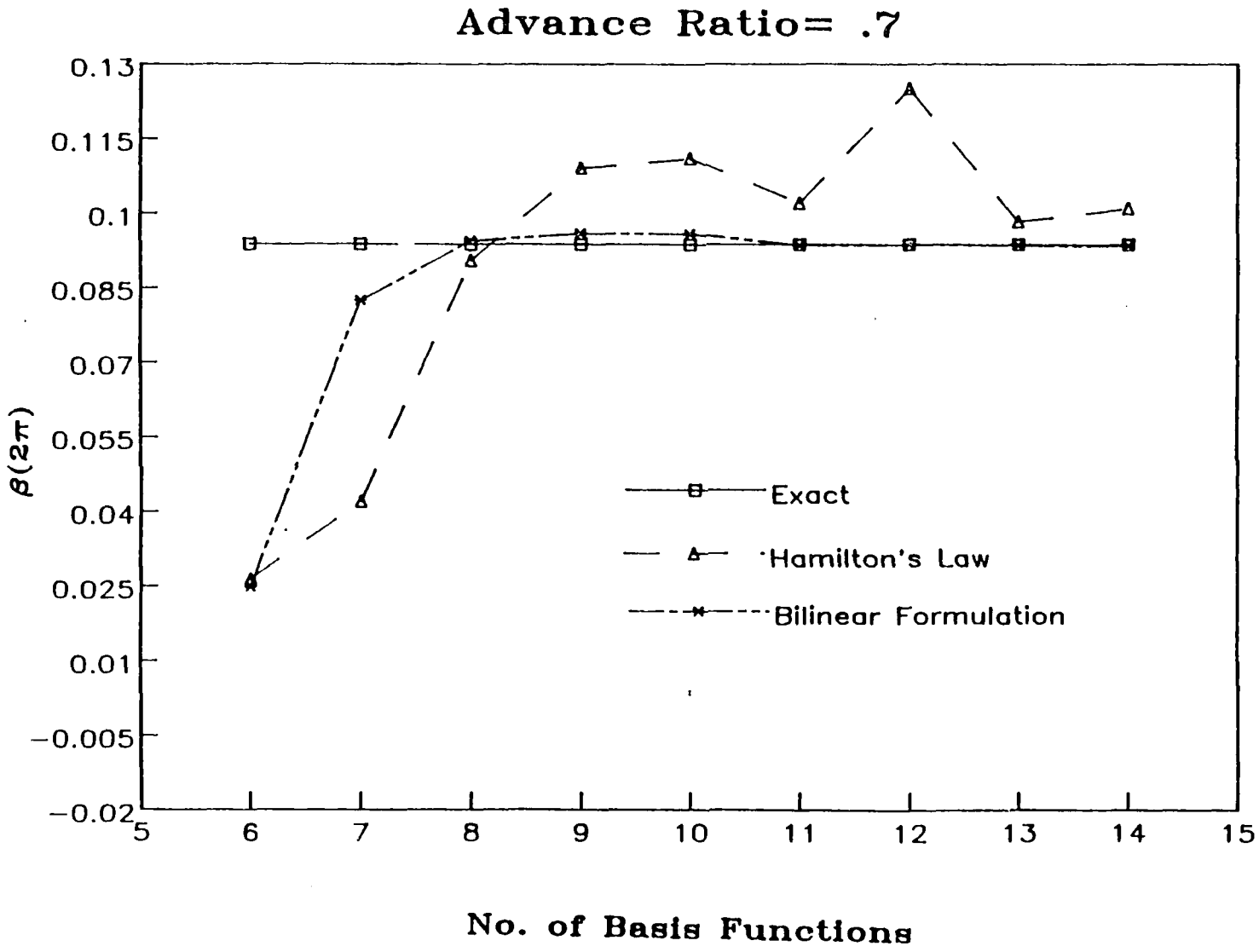

Figure 1. Flapping at the End of Period, $\mu = 0.7$

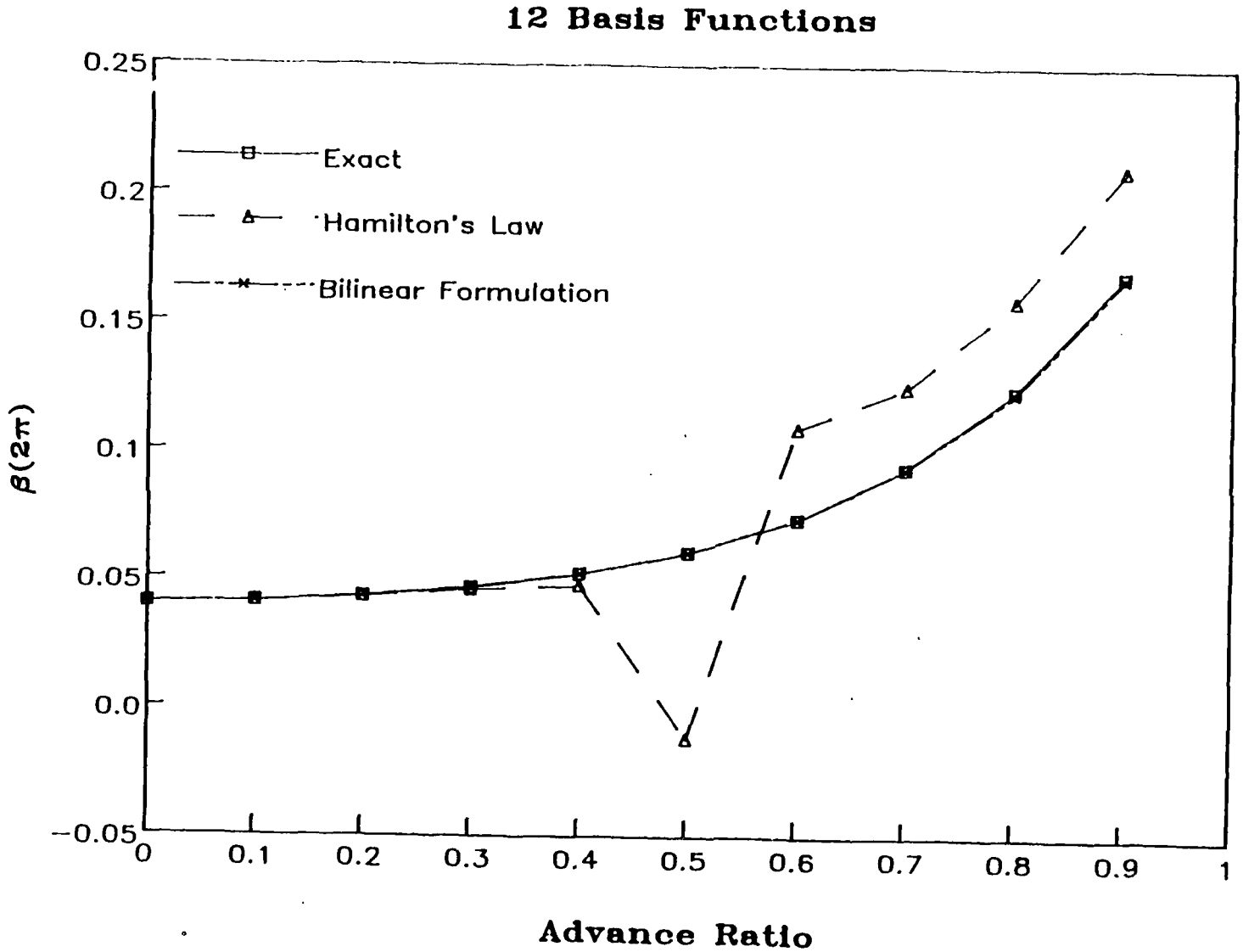

Figure 2. Flapping versus Advance Ratio, n=12

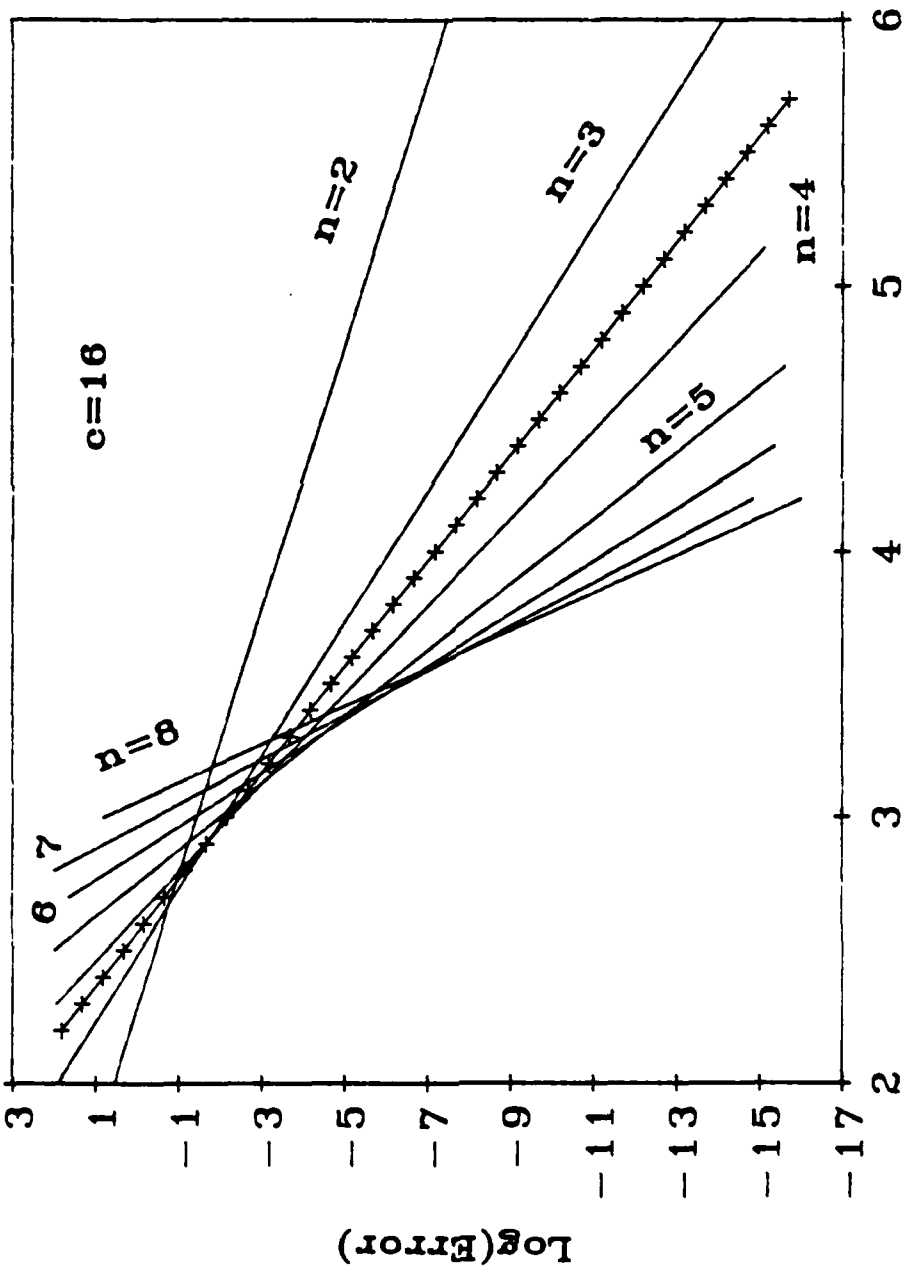

Figure 3. Error as Function of Floating-point Multiplications, c=16

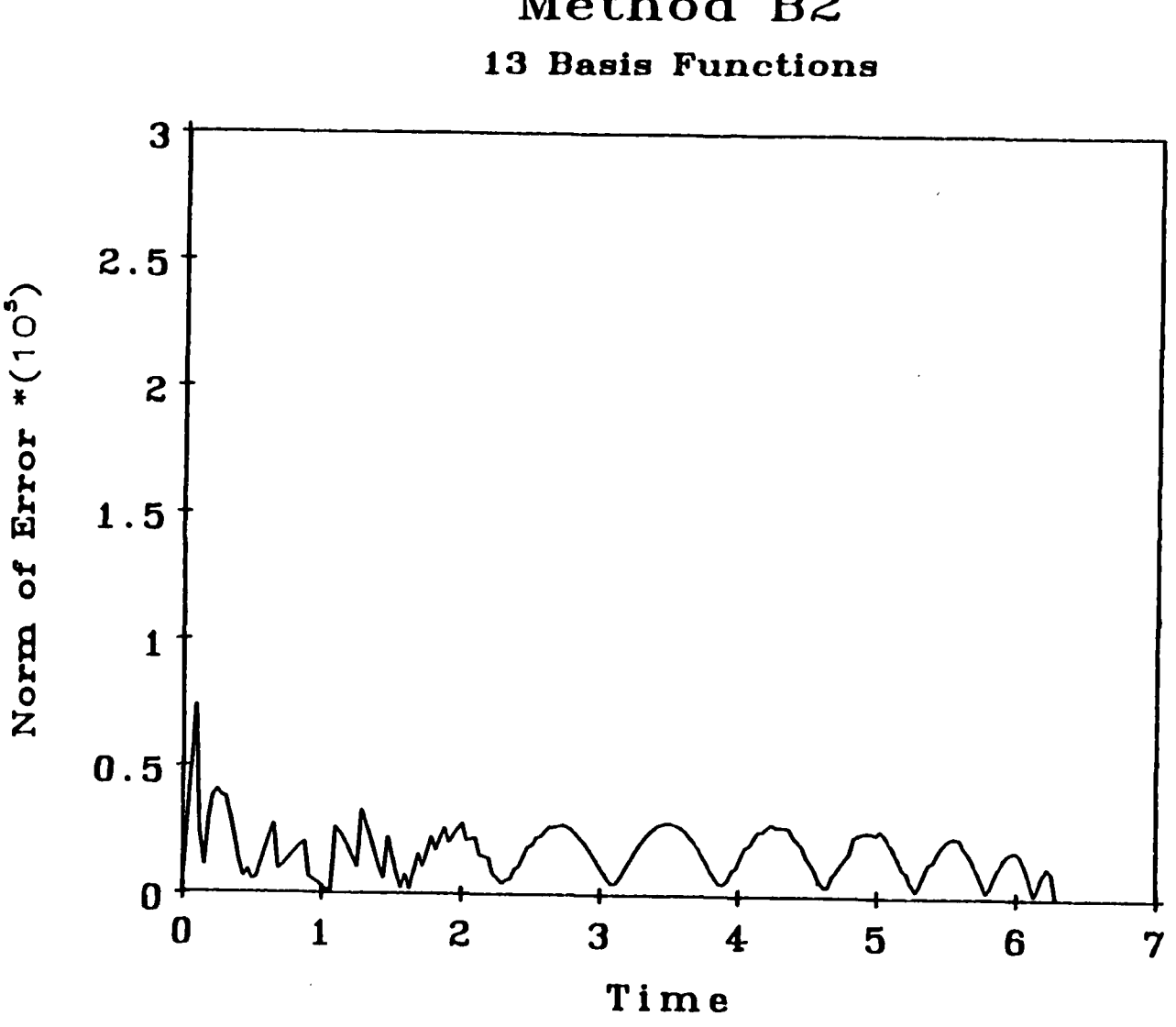

Figure 4 : Norm of Error Using Lagrange Multiplier to find $\hat{\beta}$

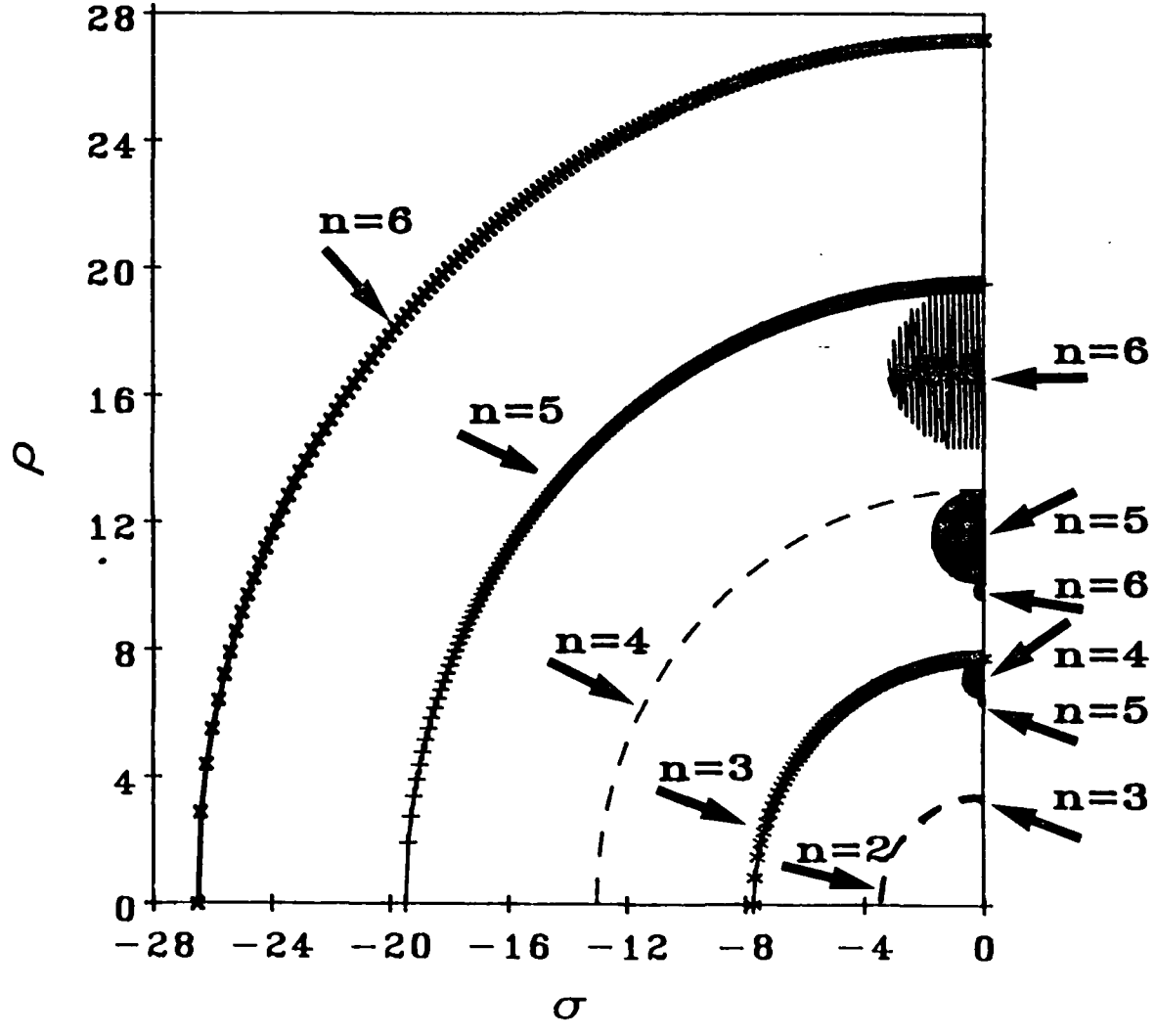

Figure 5 : Stability Boundaries of 2-6 Basis Functions

improvement. In the following, we write the system of equations to be solved including lower-order terms only

Flap equation, order ε

$$-(\tau\bar{w}^{+})^{+}+\Lambda_6\bar{w}^{++++}+\ddot{\bar{w}}=\frac{\gamma}{6a}(\bar{\Gamma}_1+\bar{\Gamma}_2)(\bar{x}+\mu\sin\psi) \tag{1}$$

Lag equation, order ε^2

$$-(\frac{1-x^2}{2}\bar{v}^{+})^{+}+\Lambda_5\bar{v}^{++++}+(\Lambda_5-\Lambda_6)(\theta+\phi)\bar{w}^{++++}-2\int_0^{\bar{x}}\bar{w}^{+}\dot{\bar{w}}^{+}d\bar{x}+\ddot{\bar{v}}-\bar{r}=$$

$$-\frac{\gamma}{6a}(\bar{\Gamma}_1+\bar{\Gamma}_2)(\bar{w}^{+}\mu\cos\psi+\bar{V}_i+\dot{\bar{w}})-\frac{\gamma}{6a}C_D(\bar{x}+\mu\sin\psi)^2 \tag{2}$$

$\bar{\Gamma}_1$ equation, order 1

$$\bar{k}\dot{\bar{\Gamma}}_1+\lambda\bar{\Gamma}_1=\lambda aU_y+\delta\bar{b}\varepsilon^{+} \tag{3}$$

$\bar{\Gamma}_2$ equation, order 1

$$\bar{k}^2\ddot{\bar{\Gamma}}_2+2dw\bar{k}\dot{\bar{\Gamma}}_2+w^2(1+d^2)\bar{\Gamma}_2=-w^2(1+d^2)[U_x\Delta C_z+e\bar{k}(\dot{U}_x\Delta C_z+\frac{\partial\Delta C_z}{\partial\theta}\dot{U}_y)] \tag{4}$$

It is interesting here to note that the terms of the lag equation are of higher order compared to the terms of the flap equation. Thus, to first order, flap drives lag in an important way, but lag has a lesser effect on flap.

An effective way of obtaining accurate pitch inputs is based on the use of an automatic feed-back system that can trim the helicopter. The auto-pilot equations are developed and expressed as follows:

$$\tau_0\ddot{\theta}_0 + \dot{\theta}_0 = A_0[\bar{C}_T - \frac{4}{3}\frac{p^2}{\gamma}\beta] \tag{5}$$

$$\tau_1\ddot{\theta}_s + \dot{\theta}_0 = A_1\frac{(p_0^2 - 1)}{\gamma}[\cos\psi - \frac{8(p^2 - 1)}{\gamma}\sin\psi]\beta \tag{6}$$

$$\tau_1\ddot{\theta}_c + \dot{\theta}_c = -A_1\frac{(p_0^2 - 1)}{\gamma}[\sin\psi + \frac{8(p^2 - 1)}{\gamma}\cos\psi]\beta \tag{7}$$

This automatic-feed-back system provides control to the helicopter for numerical purposes. It adjusts the pitch of the blade to maintain thrust, roll moment, and pitch moment. The parameters A_0 and A_1 are controller gains. The parameters τ_0 and τ_1 are time constants. The grouping $8\frac{(p^2-1)}{\gamma}$ is a coupling parameter giving the pitch-roll coupling of θ_s and θ_c. The grouping $\frac{4p^2\beta}{3\gamma}$ is an estimate of rotor thrust in the absence of an explicit C_T equation.

In the computational algorithm, input parameters define the basic aircraft configuration and flight conditions. The blade type is defined by its root stiffness, solidity, Lock number, damping, and airfoil type. Flight conditions, on the other hand, are characterized by the advance ratio, and thrust coefficient. In Table 1, we present the common parameters used in the cases discussed in this report. These parameters are selected from current helicopter data and used for illustration purposes. It is noted that we use only a constant value of C_D. In future work, we intend to include a variable C_D based on stall assumptions. Thus, the major study here is the effect of stall on lift but not on drag.

Vibration analysis includes flap and lag responses and their sensitivity to advance ratio and thrust coefficient. The torsion effect is neglected in this study. The variation of the automatic control settings required for trim is determined for a blade revolution in a steady state. In addition, the change of these settings as a response to blade stall is identified. Last, the vibration in the flap direction obtained from the stall model used in this research work is compared to results obtained when a linear aerodynamic model is used.

Table 1 Baseline Parameters

Parameter	Numerical Value	Physical Description
γ	6.63	Lock number
a	6.461	lift curve slope
C_D	.01	drag coefficient
Λ_5	.014	$\frac{EI_\zeta}{m\Omega^2R^4}$
Λ_6	.002	$\frac{EI_\zeta}{m\Omega^2R^4}$
$\bar{b}$	.05	$\frac{b}{R}$
P	1.03	flap frequency
f	.01	profile drag coefficient
σ	.1	solidity
K_β	.0203	stiffness of flap root
K_ζ	.02083	stiffness of lag root
C_ζ	.025	damping coefficent
τ_0	6.6	time constant
τ_1, τ_2	1.884	time constants
A_0	2.6	gain
A_1, A_2	3.6	gains

In order to determine the response of a helicopter blade, one must determine the pilot controls (collective pitch, cyclic pitch, and shaft tilt) that are applied to the rotor. There are two primary methods of doing this. One method is based on formulas derived by a harmonic balance of the equations without stall. In the other method, an automatic pilot is implemented to update the controls, equations (5-7). In either case, the purpose of the controller is to eliminate first harmonic moments (in the rotating frame) which come through (to the fixed frame) as steady pitching and rolling moments. In other words, "trim" implies (among other things) the balancing of these moments.

Figures 6-9 provide plots of the flapping response at $\bar{x} = 0.7$. Because this is a rigid blade with root spring, flap displacement, w, is a direct measure of root moment. The four figures show a variety of thrust coefficients and advance ratios, some with stall (high μ, high C_T), and others with little or no stall (low μ, low C_T). We see immediately that the approximate formulas for trim give a large amount of 1/rev (i.e., sin ψ) in the response. Thus, they are not accurate due to the aspects of the model neglected in such formulas (inplane motion, unsteady aerodynamics, nonuniform inflow distribution, and stall). The results with the automatic pilot, however, show two peaks per cycle, indicative of little 1/rev, mostly 2/rev, and some 3/rev, which is indicative of trim.

It is interesting that most investigations in this area have had trouble obtaining a correct trim. For example, Figure 10 shows results at $\mu = 0.4$ from Friedmann. Two different iteration schemes are used for the two plots. Notice, however, that the results (although labelled as "propulsive trim") have a large 1/rev component very similar to that seen in our approximate-formula results of Figure 6. This is to be expected because only an approximate formula is used. Figure 11 presents other results from Chopra. Here, we see a very large fore-to-aft 1/rev for a rotor supposedly in "propulsive trim" at $C_T = 0.1$, $\mu = 0.2$. Furthermore, the curves show that the response is not even periodic, as the slopes do not match at $\psi = 0°$ and 360°. In Figure 12 taken from a later Chopra reference, the authors attempt to correct the lack of trim found in Figure 11. The dashed curve is the old result (although in this paper it is corrected to be periodic), and the solid curve is the new result. In this new result, the trim solution is modified to include elastic twist. Notice, however, that although the 1/rev has been reduced by about 50%, it is still very much present. Furthermore, the solid curve is not all periodic, with an error of over 100% in the slope between $\psi = 0°$ and $\psi = 360°$. This points out the difficulties in finding a good trim solution with elastic-blade equations. The autopilot aids greatly in this regard.

In summary, unified-aerodynamic model has been introduced in the elastic-blade equations. This model is an extension of the ONERA lift model and includes plunge, unsteady free stream, and large angles of attack. An ordering scheme has been used to segregate the important terms from others. The elastic-blade equations are presented as lower-order terms and higher-order terms in the flap, lag, and circulation equations. A solution method based on a modified Galerkin's method is used to separate the time and space variables in the differential equations. A numerical solution is

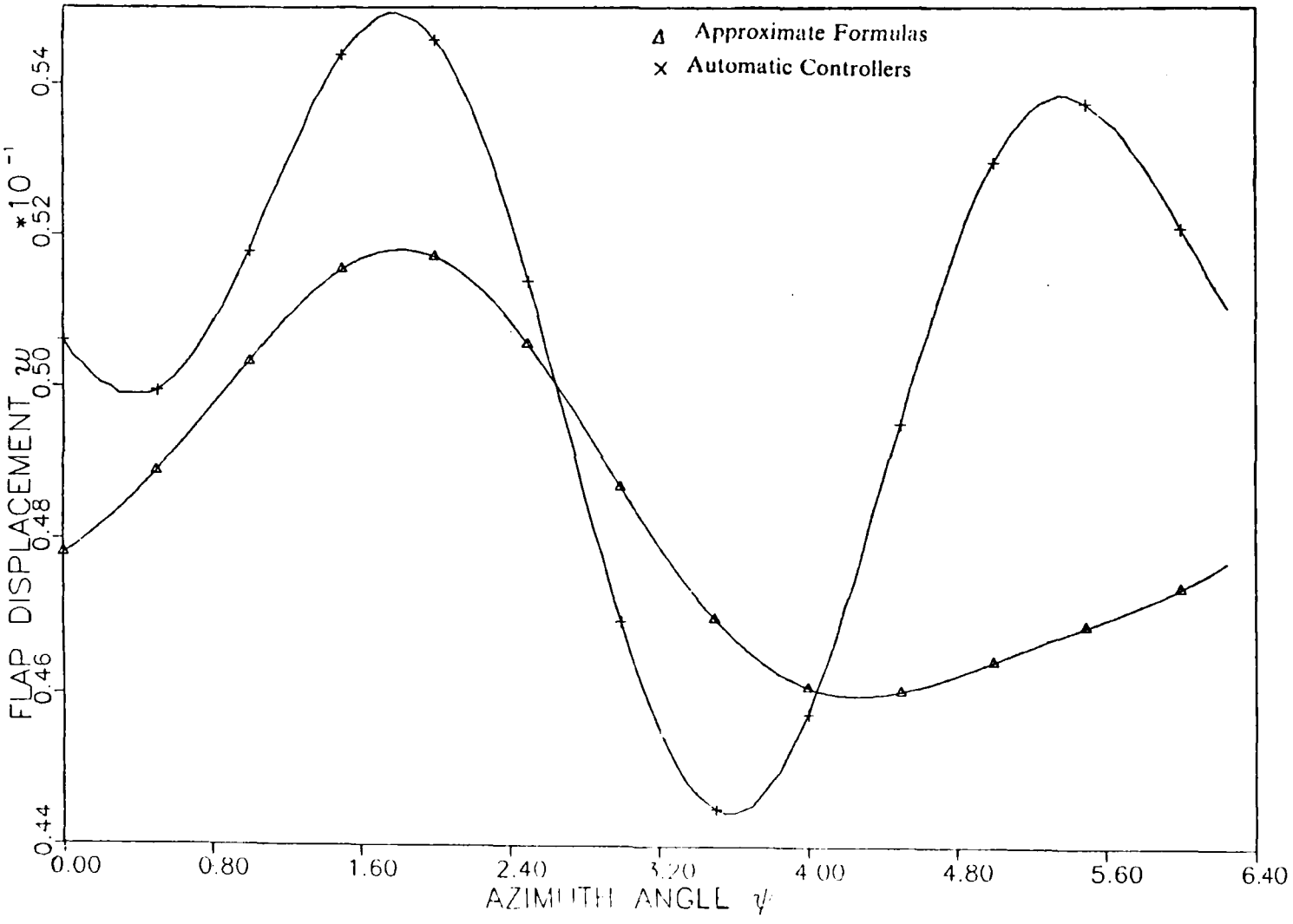

Figure 6. Effect of Trim on Flap Response

($C_T = 0.009$, $\mu = 0.10$)

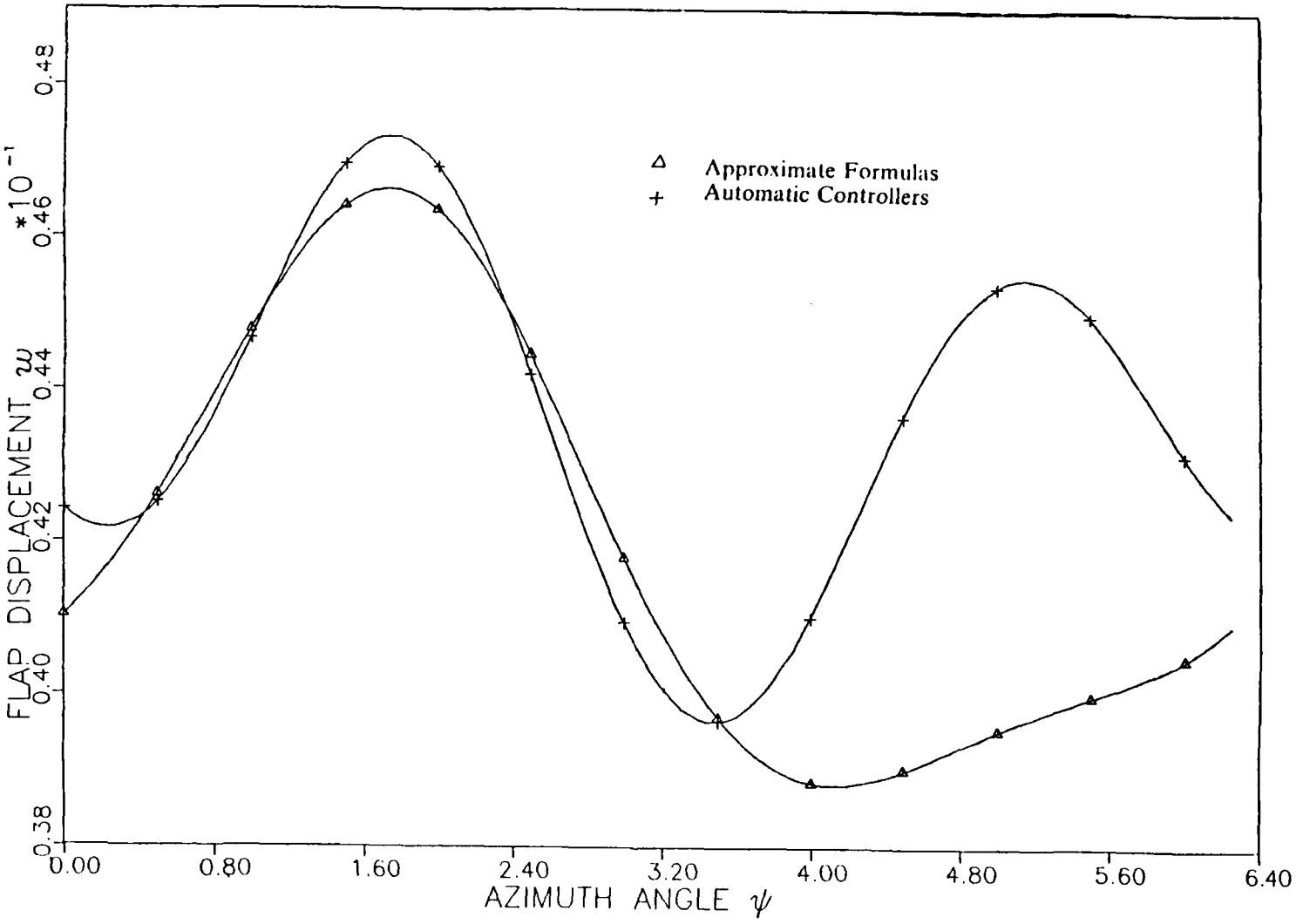

Figure 7 Effect of Trim on Flap Response

($C_T = 0.008$, $\mu = 0.15$)

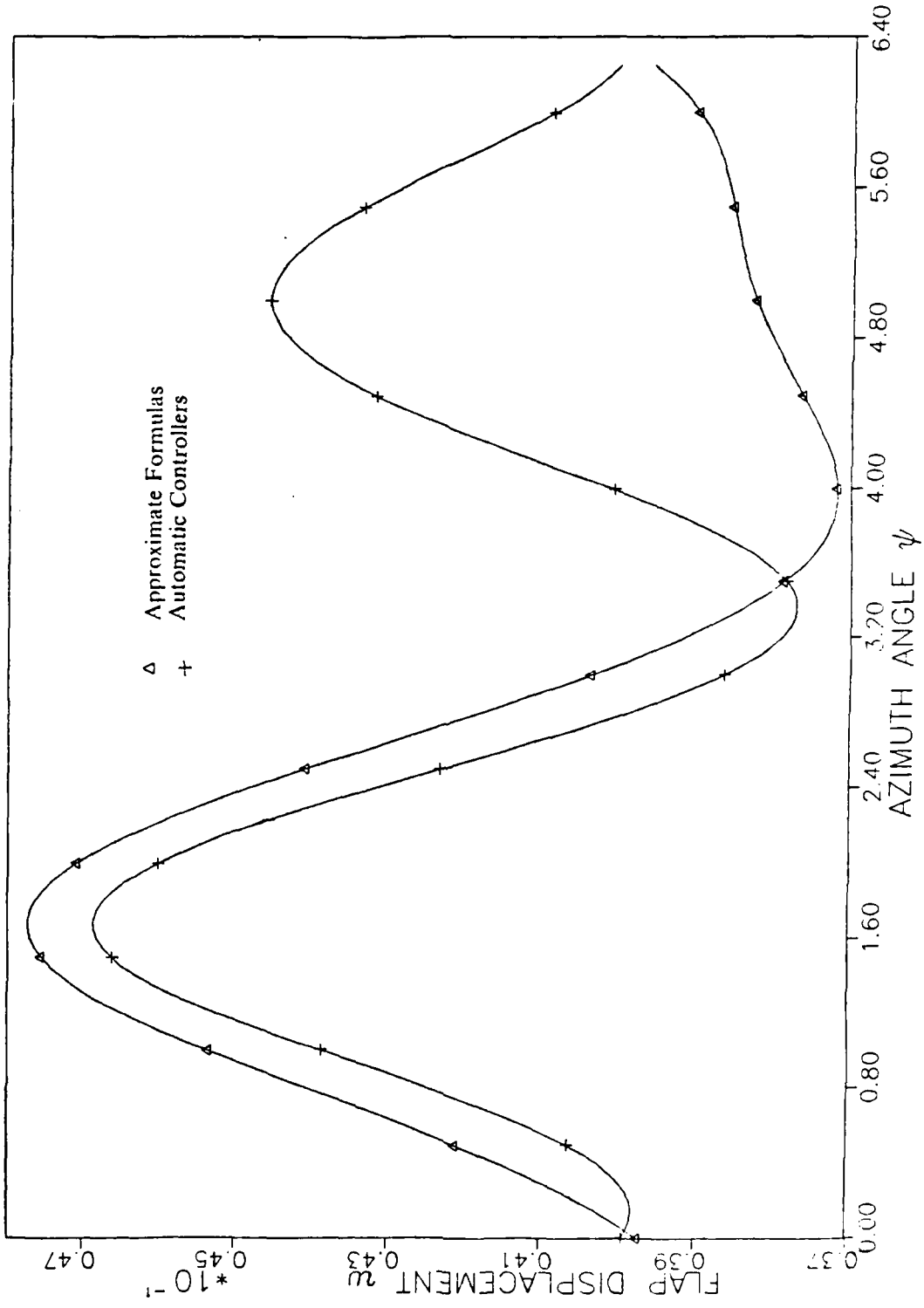

Figure 8 Effect of Trim on Flap Response

($C_T = 0.008$, $\mu = 0.20$)

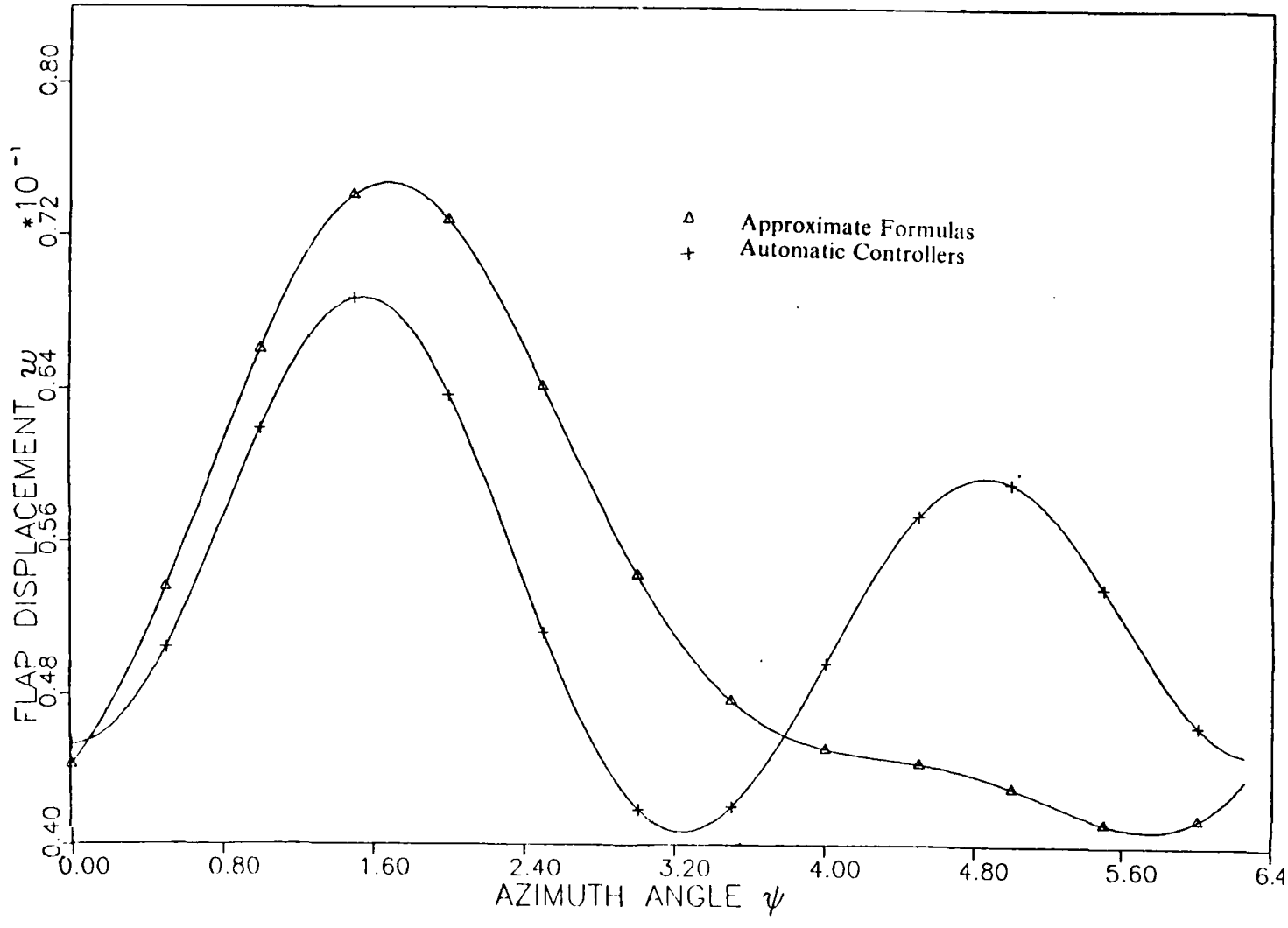

Figure 9. Effect of Trim on Flap Response

($C_T = 0.011$, $\mu = 0.3$)

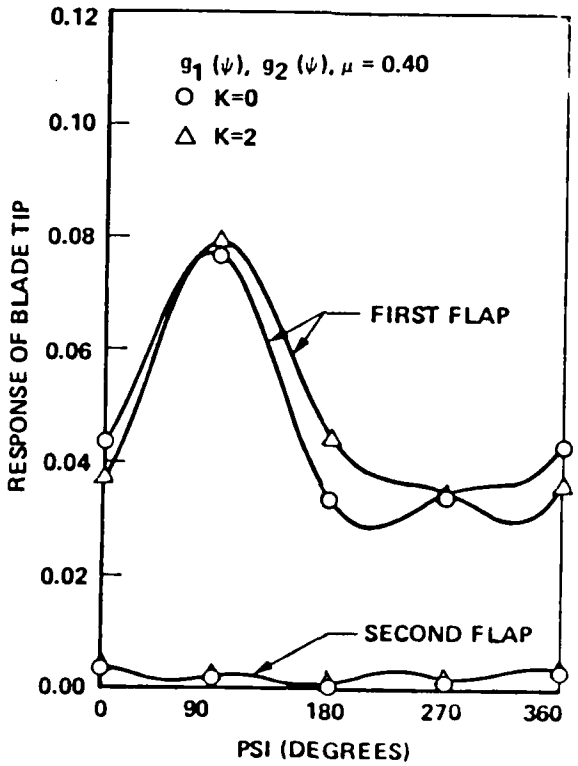

Figure 10. Soft-in-Plane Configuration, Propulsive Trim, C_T = .005, Ref.13.

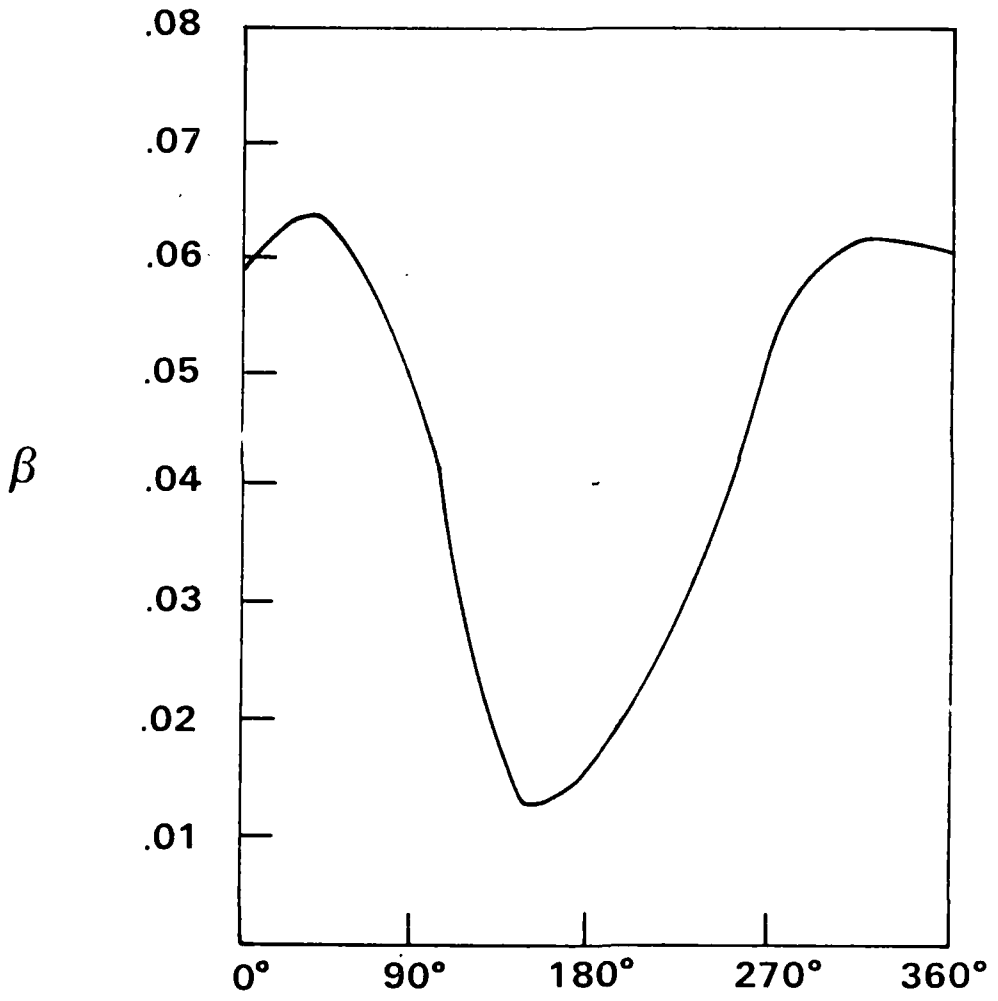

Figure 11. Flap-Lag Response, $C_T/\sigma = 0.1$, $\mu = 0.2$, Ref. 14.

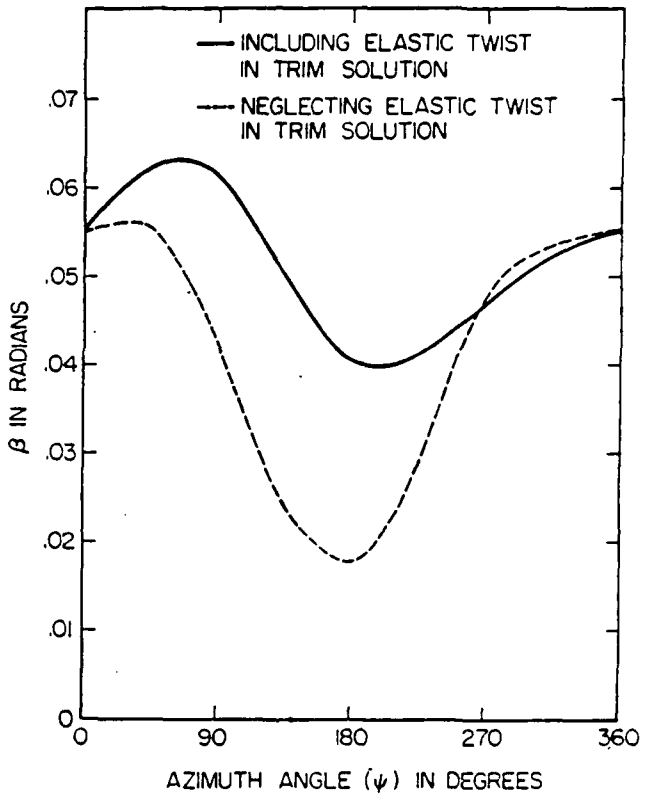

Figure 12 Flap-Lag Response

$(\frac{C_T}{\sigma} = 0.1\ ,\ \mu = 0.2)$

obtained by solving the equations for time history. Two methods have been used for trimming purposes. Dynamic response has been conducted for a variety of thrust coefficients and advance ratios. Results lead to the following conclusions:

1) The approximate method, in which pitch settings are approximated, gives large once-per-rev oscillations in the flap response.
2) Automatic controllers eliminate the once-per-rev and are used successfully beyond stall limit.

5.3 Tip-Loss Aerodynamics

In this area, we have made two very important contributions to the understanding of tip loss. First, we have developed methods to optimize the lifting-surface mesh. This optimization not only improves accuracy but also guarantees convergence, something that cannot be said of conventional mesh choices. Second, we have developed closed-form estimates of the far-wake contributions to induced velocity even with wake contraction. This improves convergence on velocity computations by a factor of 10. These two methods together from the nucleus of our tip-loss computer code which is now being utilized. Because neither of these developments has yet been published (although papers are now in review), we attach to this report an extended abstract which outlines the developments in mesh choice; and, under separate cover, we have sent to ARO a manuscript on the far-wake methodology, which has been submitted to the Journal of Aircraft.

5.4 Rotor-Body Coupling

Our research in rotor-body coupling has been severely hampered by a tragic accident involving Huang Ming-Sheng, the graduate research assistant involved in this work. Reference 8, attached to this report summarizes the basic theory behind the work, which was developed by Mr. Huang prior to his accident. Since recovering from these injuries, he has undertaken the task of coding this theory. That work is now completed. Due to the loss of time, we are not now able to deliver extensive numerical calculations as we had hoped. We will, however, continue this research (hopefully under future ARO funding).

5.5 Dynamic Inflow

We have made considerable progress in this grant toward achieving more widespread use of the theory of dynamic inflow. Reference 2 provides the ultimate correlation between our ARO-sponsored inflow model and wind-tunnel test data in the Ames 7x10 wind tunnel. Reference 3 gives a review of the past 30 years of dynamic inflow modeling including the present state of the art and current research interests. Current research interests which we have pursued in this grant are: 1) role of tip-path dynamics on actuator-disk assumptions, 2) effect of hub motions on dynamic inflow and 3) relationships between higher-harmonic dynamic inflow and unsteady aerodynamics. In the first item, we now believe that tip-path dynamics should not alter the momentum statement of dynamic-inflow theory. In the second area, hub motions can effect the formulation of linearized dynamic inflow. We have worked out

the details in Ref. 3. In item 3, we have uncovered some very strong relationships between Loewy theory and dynamic-inflow theory. Those may allow us to develop a 3-dimensional, unified theory of unsteady aerodynamics that is applicable to rotary-wing problems. An extended abstract concerning this new theory has been submitted to the AHS Forum and has been sent to ARO under separate cover.

5.6 Multiblade Transform

One of the smaller tasks in our research effort has been the study of a modified multiblade transform designed to put the differential mode into the nonrotating system. This work is essentially complete, although the student involved has not yet finished writing his M.S. thesis. The major conclusions are as follows:

1) The new transform for 2-bladed rotors does provide improvement over the conventional 2-bladed transform. In particular, it captures the essentials of the 1/rev instability at high μ.

2) For rotors with an even number of blades greater than 2(e.g., 4,6,8,etc.), there are two possible alternate transforms. One provides some improvement in the transient analysis but degrades accuracy of the forced response. The other improves forced response but degrades transients. Therefore, it is doubtful that either transform will be of general use in dynamics analyses.

3) As a spin-off of the study, we have developed matrix-manipulation algorithms that can perform the multi-blade transformation (either conventionally or in one of our new ways). These algorithms offer a simple way to make this important change of variable, and they are superior to computer algebra, numerical analysis, or fourth-order tensor approaches used by other investigators.

6. Summary of Results

In summary, we can say that our research has been very successful. It has resulted in improved analysis tools and in improved understanding of rotor vibrations. Many of these tools have been (and are being) integrated into production rotor codes.

Optimum Choice of Panel Size and Collocation Points for Rapid Convergence of Lifting-Line and Lifting-Surface Theories as Applied to Both Fixed and Rotating Aerodynamics Surfaces

by

Yihwan Danny, Chiu

Research Assistant

and

David A. Peters

Professor

School of Aerospace Engineering

Georgia Institute of Technology

Atlanta, Georgia

An Abstract Submitted to the Aerodynamics Committe of the American Helicopter Society For Presentation at the 1986 Annual National Forum.

Oct. 15, 1985

ABSTRACT

Researchers often use lifting-line and lifting-surface (or panel) theories to obtain lift and drag of fixed and rotating wings. The choice of panels, line segments, and control points within panels (i.e., collation points) is usually performed on an ad hoc basis based on engineering judgement. The results of this research show that often-used methods such as: 1) placing control points at mid-span of the panel, 2) placing large panels near the blade root and small panels near the wing tip, and 3) using equally-spaced panels near the blade tip, all result in order-unity errors in the calculation; and these errors do not decrease with refined mesh even as the number of panels and the number of significant digits is increased without bound. They are non-vanishing residuals.

The work reported here describes both how to eliminate these residual errors through proper choice of panel size and control points, and how to optimize the mesh size to give the maximum rate of convergence as the number of panels is increased. Comparisons with experimental data, with other lifting-line and lifting-surface results, and with a classical Fourier solution, demonstrate the superiority of the new procedure over conventional mesh-choice methods.

INTRODUCTION

It is commonly agreeed that the key to accurate calculation of the rotor aerodynamic behavior is the correct modeling of the rotor wake. McCroskey[1] concluded that lifting-line calculations (for rotary-wings) are in error, regardless of the wake model. The prescribed-wake method of calculation also gives errors in spanwise loading distribution, regardless of which representation is used for the surface of the blade. Even with the complicated free-wake models, lifting-surface codes still fail to predict adequately some cases with highly nonlinear twist distribution. It has been proposed that a major part of these observed discrepancies is due to improper selection of collocation points, (i.e., the possibility of running into mathematical singularities that have no physical counterpart[2]).

Most present-day rotor analyses employ a Kernel-function (in the Mangler sense), which contains a higher-order singularity and is diffcult to handle. Some researchers, however, employ the Vortex Lattice Method (VLM) which amounts to a Cauchy-type finite-element solution to both lifting-surface and lifting-line problems. Many applications of the VLM have been made to problems of the aerodynamic analysis and design of wings with considerable sucess.[3-6] However, the prediction of the detailed aerodynamic performance of a rotary wing is more difficult than that of a fixed wing. In the latter, the wake trails back from the wing in a relatively straight path to downstream infinity. The effect of the trailing vortex on the calculation can be minimized by use of certain mathematical techniques or by use of a free-wake model, which automatically allows wake roll-up. In the case of a rotary wing, the blades pass directly over their own wakes as well as those of other blades as they rotate. Furthermore, a given element has a longer residence time in the immediate vicinity of the rotor plane compared with that of a fixed-wing vortex element. Many computational efforts has been performed to reduce the error caused by wake vortex elements of rotary wings. These include the numerical integration technique[7] (for the prescribed-wake models), curved-vortex elements [8] (for free-wake models), and division of the wake into three separate regions with each computed separately.[9]

The intention of this research is to discover if a simple, systematic, optimized VLM approach can be developed for application to both fixed and rotary wings (especially for helicopter blades), despite criticisms of the VLM, which continue. These criticisms contend either that the lattics are laid out in a preconceived manner to give some desired answer or that too many lattices are required for adequate convergence of the computed loading. The present work is to derive systematically an optimized vortex-lattice layout which overcomes these objections and which can be applied to a wide variety of configuration, including rotary wings.

RECENT DEVELOPEMENTS AND SCOPE OF WORK

(A) 2-D thin airfoil theory:

In the conventional VLM, a thin airfoil is divided into a number of element panels, N, and a horseshoe vortex is placed at the 1/4 quarter-chord of each panel. The control point is located at the 3/4 quarter-chord of each panel. The results agree with Jame's[10] analysis that the first prediction-value (vortex strength) is consistently 11.4% too low for a variety of cambers. Furthermore, increasing the number of elements does not help acurracy. But C_l (lift coeff.) and C_m (pitching moment coeff.) are always exact for N greater than 2. This is the reason that the majority of aerodynamists use conventional VLM. Lan[3] developed the so-called "semi-circle rule" to select collocation points and obtain the essentially exact C_l, C_m and vortex strenth. Kocurate[11] used a Doublet-Vortex method to find the local circulation in this 2-D case and applied it to the lifting-surface performance analysis for hovering rotors. His panel spacing is biased by a cosine distribution, but control points are located at the midpoint of each panel. The method does converge as N is increased, but the rate of convergence is still too slow. Results in this paper show that the semi-circle rule can be applied to both panel size and collocation points to obtain essentially exact values of C_l, C_m, and vortex strength.

(B) Lifting line theory:

Glauert[12] solved Prandtl's lifting-line formula by using a Fourier Series method. Dejarnet[13] applied Multhopp's intepolation technique to obtain the same result as Glauert.

The conventional VLM divides the entire wing span into a number of panels, M. Also, the trailing point is located at the boundary of each panel; and the the control point is placed at the midpoint of each panel. The 1/4-3/4 rule is also used by Hough[14] to afford a singnificant reduction in computational costs. Dejoung[15] has proved that there is mathematical convergence of the VLM to the exact answer, when the 1/4-3/4 rule is used as M (or N, in 2-D case) approaches infinity. The crux of the matter lies in assessing how fast the verified 1/4-3/4 rule improves the convergence and if it is an optimized-choice. Actually, the 1/4-3/4 rule is a special case of the Finite-Difference method, for which locations presumably can be chosen arbitrarily. In this paper, however, we show that if the collocation points are laid out according to a special shape function, which has the same shape as the desired unknow circulations, then the VLM generates the fastest convergence. These shape functions must have quadradic behavior near the wing tip to match the asymptotic tip behavior[16]. Both parabolic and semi-circle functions are valid for this requirement at the tip, and these functions result in an unequally-spaced Finite-Difference technique. Results from different shape functions, compared with the classic solution for a elliptical wing, confirm the rapid convergence of the new method. A mathematical proof (of the optimality of the correct shape function) will be included in the final paper.

Basin[17] derived the mathematic equation of lifting-line theory for a rotary wing (in the prescribed-wake sense). Rosen[7] extended it to curved blades. Both of these use 10 equally-spaced meshes, but the results are not particularly accurate. Part of reason stems from the fact that M is not large enough due to poor selection of collation points. By using a semi-circle or quater-circle to select collation points, we can guarantee rapid convergence. Also included in this paper is an extension of Multhopp's interpolation technique to Prandtl's lifting formula for rotary-wing problems. This technique proves to be equivalent in accuracy to use of the "Fourier Series" method. Although based on a 3-D, rigid-wake concept, an example is given for lightly-loaded hovering blades, calculated by both Finite-Difference and Fourier Series techniques. These are compared with the experimental data[18], and both give excellent correlation.

(C) Lifting-surface theory:

The conventional VLM layout for lifting-surface theory is to use uniformly-spaced panels for both chordwise and spanwise directions over the whole wing. The 1/4-3/4 rule is also used by Hough[14] for the spanwise direction and by Belotserkovskii[6] for the chordwise direction. A reviews of these results[3-6] reveals that (M,N) should be at least (40,2) to give good convergence for typical fixed wings. Dejarnette[13] also applied Multhopp's interpolation technique to the lifting-surface formula with smaller computation time: but the method can be used only for rectangular wings. Some criteria, developed from combination of lifting-line and thin-airfoil theory, can be applied in order to select collocation points. Results in this paper show that a mesh size of only (10,2) can give excellent convergence to exact values when one uses the semi-circle rule to select panels. For rotary wings, Rosen[19] and Chang[20] use only (10,1) equally-spaced panels to calculate aerodynamics; and the results seem to be doubtful. Proper selection, made by the semi-circle or quarter-circle rule, should improve the convergence. These criteria are valid not only for VLM but also for the Double Lattice method, which is an extention of VLM.[21] For example, in the case of the propeller analysis by Murray[22], an increase in outboard unequally-spaced panels actually appears to have a detrimental effect on convergence. Thus, meshes cannot be selected or refined arbitrarily. Finally, one can reformulate the problem to solve for induced drag and pitching moment as well as for lift.

CONCLUDING REMARKS

We have reviewed the conventional VLM literature with respect to selection of collocation points and the corresponding results. These generally show a low rate of convergence. A new criteria for choice of these points is derived from lifting-line theory. A mathematical proof is provided to show that this is the optimum choice. In summary, the optimum choice of collocation points can be done as follows:

1. The choice of points in finite-difference lift calculations should be made on the

basis of equal vortex strength between points, not on equal spacing. Ideally, this would require an adaptive mesh which could change at each iteration; but practical results show this is not necessary, and a quasi-optimum mesh can be used.

2. The size of each panel must smoothly transition from large increments to small increments, moving along the direction in which the rapid change of vortex stregth occurs, and following a smooth shape function. This function must be quadratic near the tip.

3. One way to choose the points in a quasi-optimum manner is to map the spanwise and chordwise interval according to a function which has the approximate properities of criterion 1 and 2, such as a semi-circle. Both panel boundaries and collocation points must be chosen in a smooth manner according to this function.

4. A easy way to map the interval for rotary-wings in subsonic flow is to use the "Semi-circle rule". An advantage of this mapping is that integrals over the vortex strength, can often be reduced to closed form. Sevsral semi-circles can be used if several discontinuities occur.

Multhopp's interpolation technique is also specified as a semi-circle rule for unequally-spaced Finite Differences, which yields the same error as the Fourier Series method and can be applied for rotary wings. The results for wing problems by the Finite Difference technique (unequally-spaced mesh) are found to compare well with experimental data, but with smaller computational times, improved accuracy, and simplfied mathematical derivation, as compared with other continuous loading methods.

REFERENCE

1. McCroskey, W. J., "Special Opportunities in Helicopter Aerodynamics," NASA TM 84396, 1983.

2. Stepniewski, W. Z., Rotory-Wing Aerodynamics, Volume 1, Dover Publications, New York, 1981.

3. Lan, C. E., "A Quasi-Vortex-Lattice Method in Thin Wing Theory," J. Aircraft, Vol. 11, No. 9, 1974, pp. 518-527.

4. Margason, R. J. & Laman, J. E., "Vortex-Lattice Fortran Program for Estimating Subsonic Aerodynamic Characteristics of Complex Planforms," NASA TN D-6142, 1971.

5. Lamar, J. E., "A Modified Multhopp Approach for Predicting Lifting Pressures and Camber Shape for Composite Planforms in Subsonic Flow, "NASA TN D-4427, 1968.

6. Belotserkouskii, The Theory of Thin Wings in Subsonic Flow, Plenum Press, New York, 1967.

7. Rand, O. & Rosen A., "The Aerodynamics of Helicopter Rotors in Hovering and Axial Flight Using Lifting-Line Models," AE No. 485, Haifa, Israel, 1982.

8. Bliss D. B., et al., "A New Methodology For Helicopter Free Wake Analysis," 39th Annual Forum of AHS, St. Louis, May, 1983.

9. Suma, J. M. & Maskew, B., "New Methods for the Calculation of Hover Airloads," 5th European Rotorcraft and Powered Lift Aircraft Forum, Amsterdam, the Netherlands, 1979.

10. James, R. M., "On the Remarkable Accuraey for the Vortex Lattice Discretization in Thin Wing Theory," Rept DAC-67211, Douglas Aircraft Co., Long Beach, California, 1969.

11. Kocurek, J. D., A Lifting Surface Performance Analysis with Circulation Coupled Wake for Advanced Configuration Hovering Rotors, Ph. D. Thesis, Texas A&M University, May, 1978.

12. Mises, R., Theory of Flight, Dover, New York, 1959.

13. Dejarnette, F. R., "Arrangement of Vortex Lattice on Subsonic Wings," Vortex-Lattice

Utilization, NASA SP-405, 1976.

14. Hough, G. R., "Lattice Arrangements for Rapid Covergence," Vortex-Lattice Utilization, NASA SP-405, 1976.

15. Deyoung, J., "Optimum Lattice Arrangement Developed from a Rigorous Analysis Basis," Vortex-Lattice Utilization, NASA SP-405, 1976.

16. Chiu, Y. W., An Investigation of Loss of Lift and Increased Drag Near Wings Tips, M. S. Thesis, Washington University, St. Louis, May, 1984.

17. Basin, V. E., Theory of Lifting Aircrew, NASA TTF-823, 1976.

18. Meyer, J. R. & Falabella, G., "An Investigation of the Experimental Aerodynamic Loading on a Model Helicopter Rotor Blades," NASA TN 2953, 1953.

19. Rosen, A. & Graber, A., "Free Wake Model of Hovering Rotors Having Straight or Curved Blades," International Conference on Rotorcraft Basic Research, Research Triangle Park, North Carolina, Feb., 1985.

20. Chang, L. K., The Theoretical Performance of High Efficiency Propellers, Ph. D. Thesis, Purdue University, 1980.

21. Albano, E. & Rosen, W. P., "A Doublet-Lattice Method for Calculating Lift Distribution on Oscillating Surface in Subsonic Flows," AIAA Journal, Vol 7, 1969, pp. 279-285.

22. Murray, J. C. & Carta, F. O., "Lifting Surface Theory for Statically Operating Propellers," Technical Report AFAPL-TR-72-100, 1972.

COMPARISON OF 2-D THIN AIRFOIL VORTEX DISTRIBUTION WITH STRAIGHT-LINE CAMBER

$$1 = W(x) = \frac{1}{2\pi}\int_0^1 \frac{\gamma(x_1)dx_1}{x - x_1}$$

ERROR PERCENTAGE %		
Nth POINT	V.L.M.	CURRENT
1.	11.363	0.0
2.	0.897	0.0
3.	0.274	0.0003
4.	0.112	0.0001
5.	0.039	0.0001
6.	0.013	0.0001
7.	0.070	0.0006
8.	0.174	0.0001
9.	0.466	0.0005
10.	2.314	0.0034
Cl	0.0	0.0
Cm	0.0	0.0

* (10 meshes and codes)

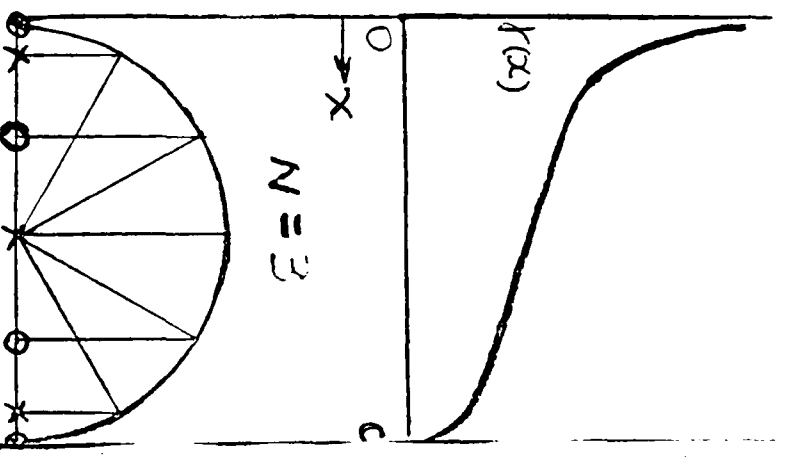

COMPARISON OF 2-D THIN AIRFOIL VORTEX DISTRIBUTION WITH PARABOLIC CAMBER

$$0.5(x-0.5) = W(x) = \frac{1}{2\pi}\int_0^1 \frac{\gamma(x_1)dx_1}{x-x_1}$$

ERROR PERCENTAGE %		
Nth POINT	V.L.M.	CURRENT
1.	11.363	0.0028
2.	0.897	0.0003
3.	0.274	0.0002
4.	0.112	0.0003
5.	0.039	0.0001
6.	0.013	0.0001
7.	0.070	0.0004
8.	0.174	0.0001
9.	0.466	0.0008
10.	2.314	0.0020
Cl	0.0	0.0
Cm	0.0	0.0

* (10 meshes and codes)

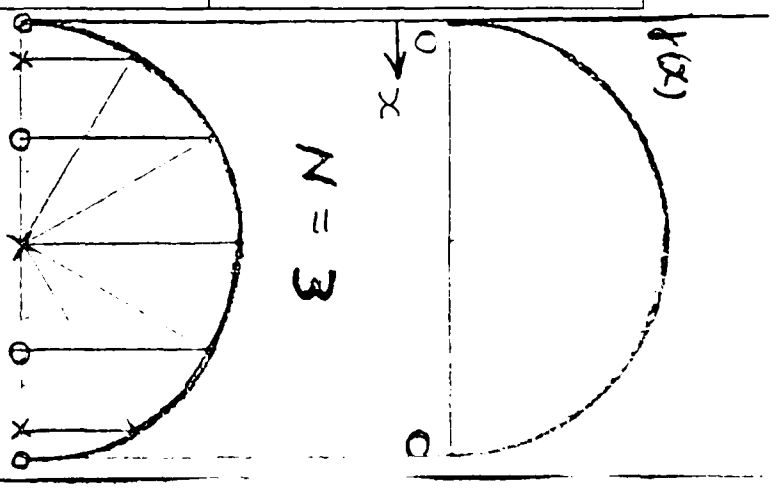

COMPARISON OF PREDICTED VORTEX DISTRIBUTIONS FOR AN AIRFOIL WITH 30% FLAP CHORD AND 30° FLAP DEFLECTION

ERROR PERCENTAGE		
NO. POINT	V.L.M.	CURRENT
1.	15.92	0.26
2.	6.25	0.29
3.	6.10	0.37
4.	6.80	0.88
5.	9.15	13.58
6.	18.24	7.38
7.	7.59	0.02
8.	11.59	0.07
Cl	4.07	0.17
Cm	2.25	0.025

* (8–(5;3)– meshes and codes)

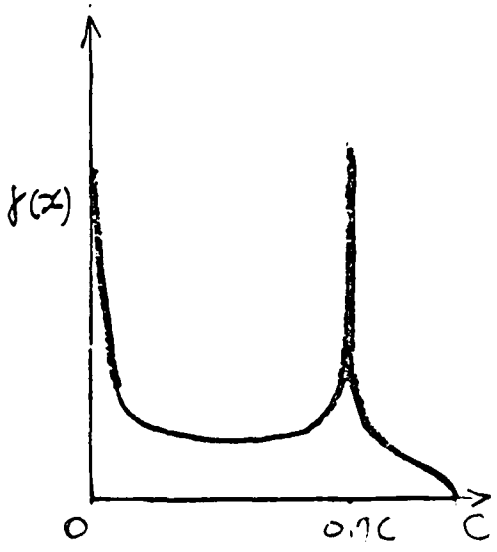

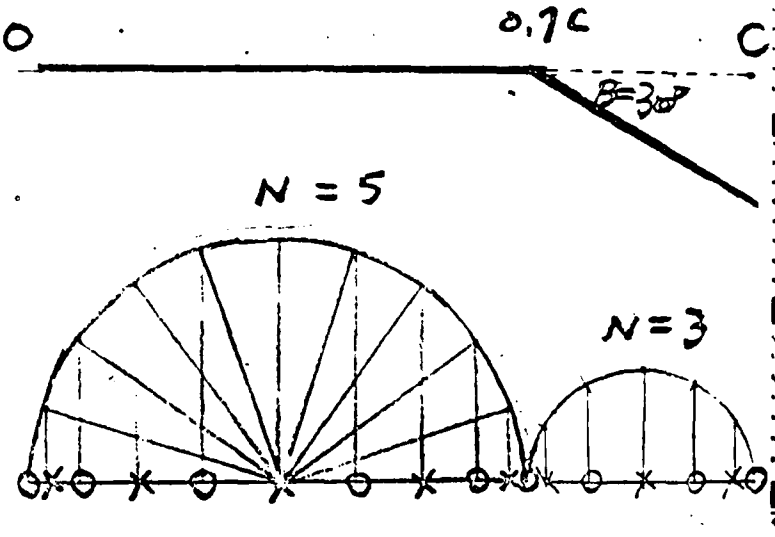

FIG. ACCURACY OF CL FOR UNTWISTED ELLIPTIC WINGS(AR=20)

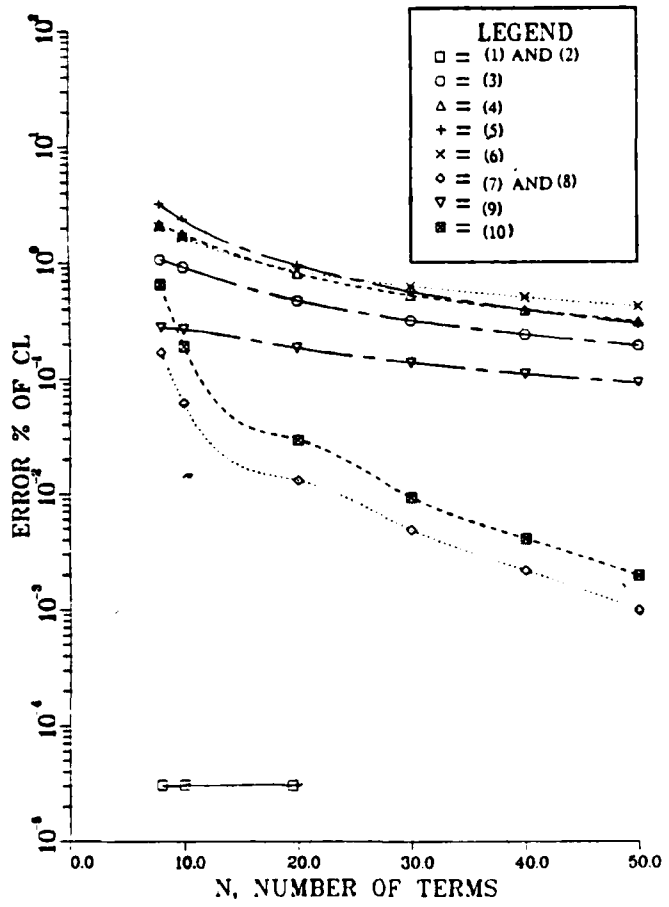

(1) FOURIER SERIES METHOD, REF 12

(2) MULTHOPP'S INTERPOLATION, REF 13

(3) Panel spacing is biased by a parabolic distribution, but control points are located at the midpoint of each panel. Also, wing tips are specified as boundary points.

(4) Panel spacing is biased by a cosine distribution, but control points are located at the midpoint of each panel. Also, wing tips are specified as boundary points.

(5) Both control and trailing points are selected according to equally-spaced panels and wing tips are specified as boundary points.

(6) Panel spacing is biased by an elliptic distribution, but control points are located at the midpoint of each panel. Also, wing tips are specified as boundary points.

(7) Both control and trailing points are selected according to the parabolic function and wing tips are specified as boundary points.

(8) Both control and trailing points are selected according to semi-circle rule and wing tips are specified as boundary points.

(9) Both control and trailing points are selected according to equally-spaced panels and wing tips are specified as trailing points.

(10) Both control and trailing points are selected according to the parabolic function and wing tips are specified as trailing points.

COMPARISON OF VORTEX DISTRIBUTION FOR A RECTANGULAR WING WITH EXPERMENTAL TESTS (Cl per degree)

AR=1.13		
METHOD	TYPE	ERROR %
MULTHOPP(20)*	L-LINE	37.00
" (10;1)*	L-SURFACE	1.80
" (10;2)*	L-SURFACE	<< 0.10
FINITE(10;2)**	L-SURFACE	0.41

AR=2.13		
METHOD	TYPE	ERROR %
MULTHOPP(20)*	L-LINE	19.00
" (10;1)*	L-SURFACE	3.90
" (10;2)*	L-SURFACE	2.30
FINITE(10;2)**	L-SURFACE	1.90

* : ref. 13

**: Current Method

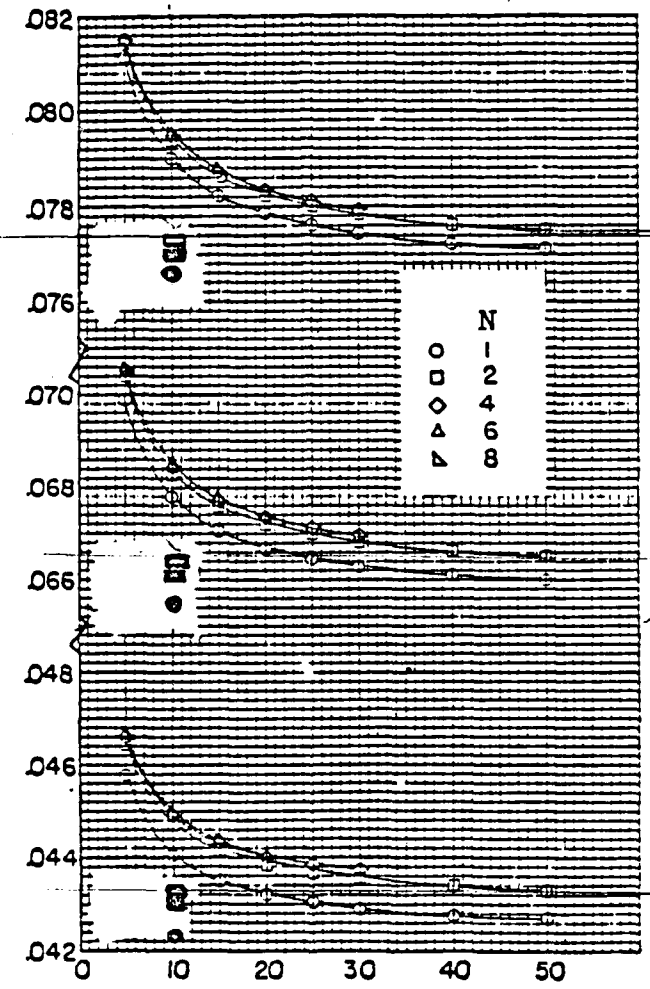

C_{L_α} (per deg.)

Number of Spanwise Vortices, M/2

. Effect of vortex-lattice arrangement for rectangular planforms.

A : Aspect Ratio

▭ : Current Method, (M,N)=(10,2)

▬ : ref. 13, (M,N)=(10,2)

● : ref. 13, (M,N)=(10,1)

——— : three conventional VLM, ref. 4

FIG. SPANWISE AERODYNAMIC LOADING

NACA0015(TN2953)

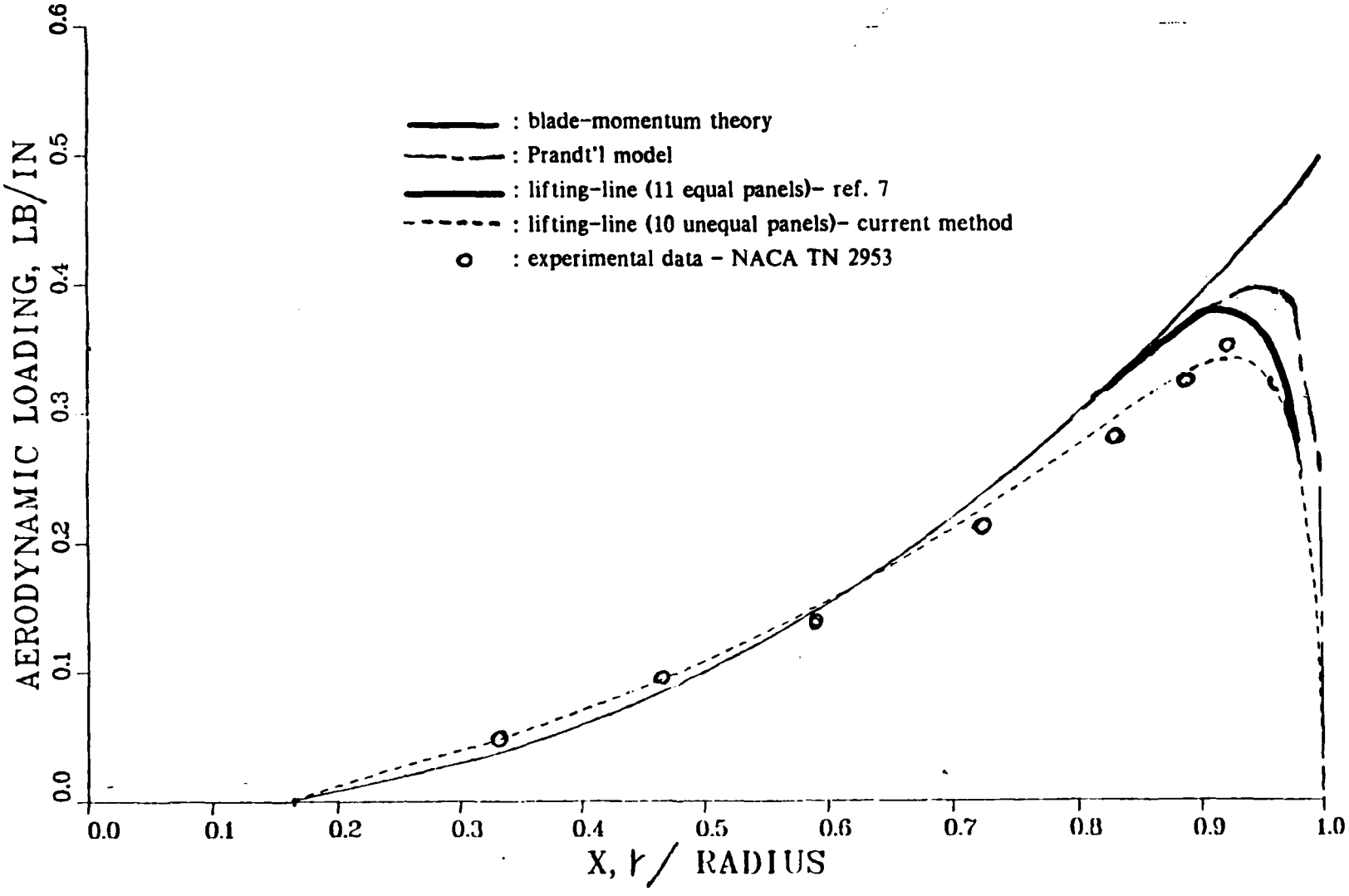

COUPLED ELASTIC ROTOR/BODY VIBRATIONS WITH INPLANE DEGREES OF FREEDOM (Work in Progress)

by

Ming-Sheng Huang
Research Assistant

and

David A. Peters
Professor of Aerospace Engineering
Georgia Institute of Technology
Atlanta, Georgia 30332

Presented at the ARO Workshop on

Dynamics and Aeroelastic Modeling

of Rotor Systems

December 4-5, 1985

INTRODUCTION

1.1 BACKGROUD

Helicopter vibration reduction is important as well as useful. With less vibration, a helicopter can survive much longer and can provide a comfortable environment for passengers. However, unlike conventional fixed-wing aircraft, the helicopter suffers an intrinsic, severe vibration source in the main rotor, which contains elastic blades and is connected flexibly to the fuselage by a hub-pylon system. So, the problem is rather sophisticated. It is well known that the fuselage motions due to rotor vibrations will cause the hub to move in all degrees of freedom. This hub motion can cause the hub loads to be different from those calculated for a fixed-hub condition. This alteration can often be an order-of-magnitude change. Therefore, in studying the effect of hub motions on hub loads, we are actually studying a feedback system.

1.2 PREVIOUS WORK

The concept of performing a coupled rotor/airframe vibration analysis by impedance matching was pointed out in 1964, Reference 1, which indicates two important facts. First, a coupled rotor/airframe analysis can be performed in a rigorous maner by separate calculation of rotor and fuselage impedances followed by a matching of forces and displacements at the hub. Second, the rotor impedance need only be calculated for a single blade and then appropriately transformed to apply to any number of blades.

In 1974, Staley and Sciarra treated the vertical vibrations of a coupled rotor and fuselage, including the effect of vertical hub motions. They used a lumped mass for rotor impedance and showed that hub motions could create order-of-magnitude changes in hub loads. In Reference 3, Hohenemser and Yin further investigate the effects of rotor-body coupling. Their model for rotor impedance is based on a rotor representation that includes two masses(each equal to one-half of the total rotor mass) connected by a spring to represent the first flapping

frequency. Reference 3 presents some very interesting conclusions that pertain to fuselage design. Particularly, it notes that under certain conditions it may be desirable to tune a fuselage frequency to the blade passage frequency in ordor to eliminate hub loads. Also, it outlines a method of computing the complete rotor impedance by finite elements and transfer matrices. Other work on the importance of hub impedance may be found in References 4-6.

Since rather crude models have been used for hub impedance (rigid mass, no aerodynamics, etc.), one might wonder why more sophisticated models were not used. The answer is straightforward. These were only the initial investigations into this effect. Furthermore, although most analysts realized the importance of detailed blade modeling for fixed hub loads (blade modes, unsteady aerodynamics, periodic coefficients, etc.), it was not clear in the beginning which of these effects would be important for finding the role of hub motion on loads. Because of the high frequencies involed (4/rev, 8/rev), many felt that inertial terms would dominate.

Reference 7 offers a sophisticated (but linear) rotor flapping model that allows for a detailed investigation of both loads and impedance (even in the presence of periodic coefficients). The method, generalized harmonic balance, involves a computer-bassed manipulation of equations that allows many degrees of freedom, many modes, and many harmonics. In Reference 8, Hsu and Peters apply this method to a flexible rotor and then use impedance matching to include plunge, pitch, and roll of the hub. This combined technique proves to be very efficient on two counts. First, the calculation for only one blade can be used for n-blades (as in Reference 1). Second, wholesale changes in fuselage properties can be made without a requirement to recalculate rotor properties. It is interesting that other investigators who began with a full-blown, coupled analysis later changed to the impedance matching technique, Reference 9-10.

For inplane vibrations with a fixed hub, Reference 8 sets up the rotor equations with rigid blades, and Reference 12 treats the same problem but with elastic blades.

In Reference 13, a fuselage model with offsets and 9 degrees of freedom is considered, coupled with a rigid inplane blade model. There is an important conclusion in reference 13 which will be very useful for further nonlinear analysis. It is that the addition of inplane degrees of freedom does not significantly affect the plunge vibrations for the cases considered, and these cases are for resonable configurations.

1.3 SCOPE OF WORK

In order to predicate the helicopter coupled vibration much better, the rotor with elastic blades should be considered. The scope of this research is to continue the previous efforts in the study of inplane coupled rotor-body vibrations. To do so, first, the dynamic partial differential equations of elastic blades including hub motions should be derived. Second, hub loads equations should be derived. Third, the fuselage equations are taken to be the same as those in Reference 13. The major goal of this research is to investigate if higher frequencies of the elastic blades will affect the coupled rotor-body vibrations.

2. ELASTIC BLADE EQUATIONS

The equations of motion for a flexible hingeless rotor blade in forward flight, as derived in Reference 12, are the starting point for this analysis. The present analysis, however, expands the previous work in following way. The hub motions (including plunge, longitudinal and lateral displacements, pitch and roll angles, and their first and second derivatives) are added to the equations.

2.1 COORDINATES AND THEIR TRASFORMATIONS

The coordinate systems used in the present analysis are shown in Figure 1. The triplet X,Y,Z represents a fuselage fixed coordinate system; and the triplet x,y,z represents a rotating coordinate system. Between the Z and z axes there is a precone angle. The deflection components of the elastic axis of the deformed blade (u, v, and w) are taken in the x,y,z coordinate system. The final set of axes, x', y', z' are taken along the deformed axes.

There are transformations among these coordinates. Figure 2 shows the pitch angle α_c and roll angle α_s; and, Figure 3 indicates azimuth angle ψ and precone angle β_{pc}. With these angles, one can trasform any vector, say $\vec{F}$, from the fixed coordinate X,Y,Z to the undeformed rotating coordinate x,y,z. We have:

$$\begin{pmatrix} F_x \\ F_y \\ F_z \end{pmatrix} = [T_R] \begin{pmatrix} F_X \\ F_Y \\ F_Z \end{pmatrix} \tag{1}$$

where,

$$[T_R] = \begin{pmatrix} \begin{pmatrix} \cos\beta_{pc}\cos\alpha_c\cos\psi \\ +\sin\beta_{pc}\sin\alpha_c \end{pmatrix} & \begin{pmatrix} -\cos\beta_{pc}\cos\psi\sin\alpha_c\sin\alpha_s \\ +\cos\beta_{pc}\sin\psi\cos\alpha_s \\ +\sin\beta_{pc}\cos\alpha_c\sin\alpha_s \end{pmatrix} & \begin{pmatrix} -\cos\beta_{pc}\cos\psi\sin\alpha_c\cos\alpha_s \\ -\cos\beta_{pc}\sin\psi\sin\alpha_s \\ +\sin\beta_{pc}\cos\alpha_c\cos\alpha_s \end{pmatrix} \\ \\ (-\sin\psi\cos\alpha_c) & \begin{pmatrix} \sin\psi\sin\alpha_c\sin\alpha_s \\ +\cos\psi\cos\alpha_s \end{pmatrix} & \begin{pmatrix} \sin\psi\sin\alpha_c\cos\alpha_s \\ -\cos\psi\sin\alpha_s \end{pmatrix} \\ \\ \begin{pmatrix} -\sin\beta_{pc}\cos\psi\cos\alpha_c \\ +\cos\beta_{pc}\sin\alpha_c \end{pmatrix} & \begin{pmatrix} \sin\beta_{pc}\cos\psi\sin\alpha_c\sin\alpha_s \\ -\sin\beta_{pc}\sin\psi\cos\alpha_s \\ +\cos\beta_{pc}\cos\alpha_c\sin\alpha_s \end{pmatrix} & \begin{pmatrix} \sin\beta_{pc}\cos\psi\sin\alpha_c\cos\alpha_s \\ +\sin\beta_{pc}\sin\psi\sin\alpha_s \\ +\cos\beta_{pc}\cos\alpha_c\cos\alpha_s \end{pmatrix} \end{pmatrix} \tag{2}$$

The transformation from undeformed coordinates to deformed coordinates is given by

$$\begin{pmatrix} F_{x'} \\ F_{y'} \\ F_{z'} \end{pmatrix} = [T_d] \begin{pmatrix} F_x \\ F_y \\ F_z \end{pmatrix} \tag{3}$$

where,

$$[T_d] = \begin{pmatrix} 1 & v^+ & w^+ \\ -\theta w^+ - v^+ & 1 & \theta \\ -w^+ + \theta v^+ & -\theta - w^+ v^+ & 1 \end{pmatrix} \tag{4}$$

With these transformations, we can transfer the vectors to any coordinates needed. Other, kinematic contributions to θ are treated as pitch-lag coupling.

2.2 HAMILTON'S LAW

The next step in the derivation is to apply Hamilton's Law to obtain equations of motion. The Hamilton's Law can be expressed as

$$\int_{t_1}^{t_2} (\delta U - \delta T - \delta W)\, dt + \frac{\partial T}{\partial \dot{q}_i} \delta q_i \Big|_{t_1}^{t_2} = 0 \tag{5}$$

where, δU and δT are the variations in strain energy and kinetic energy, and δW is the virtual work. 'q_i' is the generalized coordinate. To apply equation (5), δU, δT and δW must be formulated in terms of the generalized coordinates.

2.2.1 STRAIN ENERGY

The strain energy can be expressed as follows:

$$U = \frac{1}{2} \int_0^R \iint_A E \epsilon_{xx}^2 dA\, dx \tag{6}$$

then,

$$\delta U = \int_0^R \iint_A E \epsilon_{xx} \delta \epsilon_{xx}\, dA\, dx \tag{7}$$

where,

$$\epsilon_{xx} = u' + \frac{v'^2}{2} + \frac{w'^2}{2} - v''[\eta \cos\theta_e - \varsigma \cos\theta_e] - w''[\eta \sin\theta_e + \varsigma \cos\theta_e] \tag{8}$$

and

$$\theta_e = R_e\theta \tag{9}$$

Therefore, δU can be fuether expressed as

$$\delta U = \int_0^R \Big\{ V_{x'}[\delta u' + v'\delta v' + w'\delta w'] + [M_{z'} + M_{y'}R_e\theta]\delta V'' + [M_{z'}R_e\theta - M_{y'}]\delta W'' \Big\}\, dx \tag{10}$$

where,

$$V_{x'} = EA\left\{ u' + \frac{v'^2}{2} + \frac{w'^2}{2} \right\} \tag{11}$$

$$M_{y'} = EI_{y'}[v''R_e\theta - w''] \tag{12}$$

$$M_{z'} = EI_{z'}[v'' + w''R_e\theta] \tag{13}$$

Integration by parts of δU gives the following result:

$$\delta U = \int_0^R \left(\bar{Y}_u\delta u + \bar{Y}_v\delta v + \bar{Y}_w\delta w\right) dx + b(U) \tag{14}$$

where,

$$\bar{Y}_u = -(V_{x'})' \tag{15}$$

$$\bar{Y}_v = [M_{z'} + M_{y'}R_e\theta]'' - (V_{x'}v')' \tag{16}$$

$$\bar{Y}_w = [M_{z'}R_e\theta - M_{y'}]'' - (V_{x'}w')' \tag{17}$$

and the boundary condition is

$$b(U) = V_{x'}\delta u\Big|_0^R + \Big\{ V_{x'}v' - [M_{z'} + M_{y'}R_e\theta]' \Big\}\delta v\Big|_0^R + [M_{z'} + M_{y'}R_e\theta]\delta v'\Big|_0^R + \Big\{ V_{x'}w - [M_{z'}R_e\theta - M_{y'}]' \Big\}\delta w\Big|_0^R + [M_{z'}R_e\theta - M_{y'}]\delta w'\Big|_0^R \tag{18}$$

2.2.2. KINETIC ENERGY

The kinetic energy can be expressed as

$$T = \frac{1}{2}\int_0^R \iint_A \rho \vec{V} \cdot \vec{V}\, d\eta\, d\varsigma\, dx \tag{19}$$

and the variation is

$$\delta T = \int_0^R \iint_A \rho \vec{V} \cdot \delta\vec{V}\, d\eta\, d\varsigma\, dx \tag{20}$$

where the velocity vector is

$$\begin{aligned}
\vec{V} = \vec{i}\Big\{ & \dot{x}_1 + \dot{\alpha}_s z_1 \sin\psi + \dot{\alpha}_c z_1 \cos\psi - \dot{\alpha}_s y_1 \beta_{pc} \cos\psi \\
& + \dot{\alpha}_c y_1 \beta_{pc} \sin\psi - \Omega y_1 - \dot{X}\cos\psi + \dot{Y}\sin\psi - \dot{Z}\beta_{pc}\Big\} \\
+ \vec{j}\Big\{ & \dot{y}_1 + \dot{\alpha}_s z_1 \cos\psi - \dot{\alpha}_c z_1 \sin\psi - \Omega z_1 \beta_{pc} + \dot{X}\sin\psi \\
& + \dot{\alpha}_s x_1 \beta_{pc} \cos\psi - \dot{\alpha}_c x_1 \beta_{pc} \sin\psi + \Omega x_1 + \dot{Y}\cos\psi\Big\} \\
+ \vec{k}\Big\{ & \dot{z}_1 - \dot{\alpha}_s y_1 \cos\psi + \dot{\alpha}_c y_1 \sin\psi + \Omega y_1 \beta_{pc} - \dot{\alpha}_s x_1 \sin\psi \\
& - \dot{\alpha}_c x_1 \cos\psi + \dot{X}\beta_{pc}\cos\psi - \dot{Y}\beta_{pc}\sin\psi - \dot{Z}\Big\}
\end{aligned} \tag{21}$$

and where,

$$\begin{aligned}
x_1 &= x + u - v'[\eta\cos\theta - \varsigma\sin\theta] - w'[\eta\sin\theta + \varsigma\cos\theta] \\
y_1 &= v + \eta\cos\theta - \varsigma\sin\theta \\
z_1 &= w + \eta\sin\theta + \varsigma\cos\theta
\end{aligned} \tag{22}$$

After integration over the blade cross section, the variation of kinetic energy becomes:

$$\delta T = \int_0^R \left(\bar{Z}_u \delta u + \bar{Z}_v \delta v + \bar{Z}_w \delta w + \bar{Z}_{v'} \delta v' + \bar{Z}_{w'} \delta w'\right) dx \tag{23}$$

where,

$$\begin{aligned}
Z_u = m\big[& \ddot{u} - \dot{\alpha}_s \dot{w}\sin\Omega t + 2\Omega\dot{v} + \ddot{X}\cos\Omega t - \ddot{Y}\sin\Omega t - \Omega\dot{\alpha}_c\dot{w}\sin\Omega t \\
& + 2\Omega\dot{\alpha}_s\beta_{pc}x\cos\Omega t - 2\Omega\dot{\alpha}_c\beta_{pc}x\sin\Omega t + \Omega\dot{\alpha}_s\dot{w}\cos\Omega t
\end{aligned}$$

$$+\Omega^2 x - \dot{\alpha_s}\dot{w}\sin\Omega t + \dot{\alpha_s}^2 x + 2\dot{\alpha_s}\dot{\alpha_c}x\cos\Omega t\sin\Omega t$$

$$-\dot{\alpha_c}\dot{w}\cos\Omega t - \bar{Z}\beta_{pc} + \dot{Z}\dot{\alpha_s}\sin\Omega t + \dot{Z}\dot{\alpha_c}\cos\Omega t]$$

$$+m(w+e\sin\theta)[-\bar{\alpha_s}\sin\Omega t - \Omega\dot{\alpha_s}\cos\Omega t - \Omega^2\beta_{pc}] \tag{24}$$

$$\bar{Z}_v = m[-\bar{v} + 2\dot{\alpha_c}\dot{w}\sin\Omega t + \Omega\beta_{pc}\dot{w} - \bar{\alpha_s}\beta_{pc}x\cos\Omega t + \dot{\alpha_s}\Omega\beta_{pc}x\sin\Omega t$$

$$+\bar{\alpha_c}\beta_{pc}x\sin\Omega t + \dot{\alpha_c}\beta_{pc}x\cos\Omega t - \bar{X}\sin\Omega t - \bar{Y}\cos\Omega t - 2\dot{\alpha_s}\dot{w}\cos\Omega t$$

$$+\dot{\alpha_s}^2 x\sin\Omega t\cos\Omega t - \dot{\alpha_c}\dot{alpha_s}(\cos^2\Omega t - \sin^2\Omega t) - \dot{\alpha_c}^2 x\sin\Omega t\cos\Omega t$$

$$+\Omega\beta_{pc}\dot{w} - \Omega\dot{\alpha_s}\beta_{pc}x\sin\Omega t - \Omega\dot{\alpha_c}\beta_{pc}x\cos\Omega t + \dot{Z}\dot{\alpha_s}\cos\Omega t - \dot{Z}\dot{\alpha_c}\sin\Omega t]$$

$$+m\Omega^2(v+e\cos\theta) - 2\Omega m\dot{u} + 2me\Omega(\dot{v'}\cos\theta + \dot{w'}\sin\theta)$$

$$+m(w+e\sin\theta)[-\bar{\alpha_s}\cos\Omega t + \bar{\alpha_c}\sin\Omega t] \tag{25}$$

$$\bar{Z}_w = m[-\bar{w} + 2\dot{\alpha_s}\dot{v}\cos\Omega t - 2\dot{\alpha_c}\dot{v}\sin\Omega t - 2\Omega\beta_{pc}\dot{v} + \bar{\alpha_s}x\sin\Omega t + 2\dot{\alpha_s}\Omega x\cos\Omega t$$

$$+\bar{\alpha_c}x\cos\Omega t - 2\Omega\dot{\alpha_c}x\sin\Omega t + \dot{Y}\dot{\alpha_s} + \bar{X}\beta_{pc}\cos\Omega t - \bar{Y}\beta_{pc}\sin\Omega t$$

$$-\bar{Z} - \dot{\bar{X}}\dot{alpha_c} - \Omega^2\beta_{pc}x - 2\Omega\bar{X}\beta_{pc}\sin\Omega t - 2\Omega\dot{Y}\beta_{pc}\cos\Omega t$$

$$+m(v+e\cos\theta)[\bar{\alpha_s}\cos\Omega t - 2\Omega\dot{\alpha_s}\sin\Omega t - \bar{\alpha_c}\sin\Omega t - 2\Omega\dot{\alpha_c}\cos\Omega t] \tag{26}$$

$$\bar{Z}_{v'} = me\cos\theta[\bar{Y}\sin\Omega t - \bar{X}\cos\Omega t - \Omega^2 x - 2\Omega\dot{v}] \tag{27}$$

$$\bar{Z}_{w'} = me\sin\theta[\bar{Y}\sin\Omega t - \bar{X}\cos\Omega t - \Omega^2 x - 2\Omega\dot{v}] \tag{28}$$

in which,

$$m = \iint_A \rho\, d\eta\, d\zeta \tag{29}$$

$$me\cos\theta = \iint_A \rho(y_1 - v)\, d\eta\, d\zeta \tag{30}$$

$$me\sin\theta = \iint_A \rho(z_1 - w)\, d\eta\, d\zeta \tag{31}$$

Integration by parts again gives

$$\int_0^R \bar{Z}_{v'}\delta v'\, dx = \int_0^R \bar{Z}_{v'}\delta(\delta v)$$

$$= \bar{Z}_{v'}\delta v\Big|_0^R - \int_0^R \bar{Z}'_{v'}\delta v\, dx \tag{32}$$

and

$$\int_0^R Z_{w'}\delta w'\,dx = \bar{Z}_{w'}\delta w\Big|_0^R - \int_0^R \bar{Z}'_{w'}\delta w\,dx \tag{33}$$

Finally, the variation of kinetic energy can be expressed as

$$\delta T = \int_0^R [\bar{Z}_u\delta u + (bar Z_v - \bar{Z}'_{v'})\delta v + (\bar{Z}_w - \bar{Z}'_{w'})\delta w]\,dx + b(T) \tag{34}$$

where the boundary condition is

$$b(T) = \bar{Z}_{v'}\delta v\Big|_0^R + \bar{Z}_{w'}\delta w\Big|_0^R \tag{35}$$

2.2.3 VIRTUAL WORK

The final step necessary to compute the equations is the computation of virtual work. The virtual work, δW, is mainly due to the nonconservative external forces which come from the theory of aerodynamics. The virtual work can be expressed as

$$\delta W = \int_0^R (L_u\delta u + L_v\delta v + L_w\delta w)\,dx \tag{36}$$

where L_u, L_v, L_w are forces acting along x,y,z directions.

2.2.4 GENERAL EQUATIONS

The functional of Hamilton's Law has three variables u, v, and w. This will lead to three Euler-Lagrange equations which are the required equations of motion. Later, u can be eliminated which will reduce the system of equations to only two. The basic equations come from Equation (5). If we ignore the trailing terms that are cancelled by

$$\delta q_i\Big|_{t_1}^{t_2} = 0 \tag{37}$$

then we have

$$\int_{t_1}^{t_2} (\delta U - \delta T - \delta W)\,dt = 0 \tag{38}$$

Therefore,

$$\delta U - \delta T - \delta W = 0 \tag{39}$$

with trailing terms dropped. In the case considered, we have

$$\int_0^R \left\{(\bar{Y}_u - \bar{Z}_u - L_u)\delta u + [\bar{Y}_v - (\bar{Z}_v - \bar{Z}'_{v'}) - L_v]\delta v + [\bar{Y}_w - (\bar{Z}_w - \bar{Z}'_{w'}) - L_w]\delta w\right\} d\bar{x} + b(U) - b(T) = 0 \quad (40)$$

From the principles of variational calculus, the equations of motion and boundary conditions can be obtained from Equation (40).

δU equations:

$$\bar{Y}_u - \bar{Z}_u = L_u \quad (41)$$

δV equations:

$$\bar{Y}_v - (\bar{Z}_v - \bar{Z}'_{v'}) = L_v \quad (42)$$

δW equations:

$$\bar{Y}_w - (\bar{Z}_w - \bar{Z}'_{w'}) = L_w \quad (43)$$

and boundary condition:

$$b(U) - b(T) = 0 \quad (44)$$

2.2.5 BASIC EQUATIONS

With the help of the ordering scheme in Reference 12, but keeping flapping equations o(ϵ), lead-lag equation o(ϵ^2), and eliminating axial deflection from δU equation, we obtain flapping and lead-lag equations in nondimensional form as follows:

Flapping equation:

$$\begin{aligned}&\Lambda_1^2\bar{w}^{++++} + (\Lambda_2^2 - \Lambda_1^2)R_e\theta\bar{v}^{++++} - \tau^+\bar{w}^+ - \tau\bar{w}^{++} + \bar{w}^{**} - 2\bar{v}^{*+} - \alpha_s^{**}\bar{x}\sin\psi \\ &- 2\alpha_s^*\bar{x}\cos\psi - \alpha_c^{**}\cos\psi + 2\alpha_c^*\bar{x}\sin\psi + \bar{X}^{**}\beta_{pc}\cos\psi - \bar{Y}^{**}\beta_{pc}\sin\psi - \bar{Z}^{**} + \beta_{pc}\bar{x} \\ &= L_w \end{aligned} \quad (45)$$

Lead-lag equation

$$\begin{aligned}&\Lambda_2^2\bar{v}^{++++} + (\Lambda_2^2 - \Lambda_1^2)R_e\theta barw^{++++} - \tau^+\bar{v}^+ - \tau\bar{v}^{++} - \bar{v} - 2\int_0^{\bar{x}} \bar{w}^+\bar{w}^{*+}\,d\bar{x} \\ &+ \bar{v}^{**} - \alpha_c^{**}\beta_{pc}\sin\psi - \alpha_c^{**}\bar{x}\bar{w}\sin\psi + \alpha_c^{*2}\bar{x}\sin\psi\cos\psi - 2\alpha_c^*\bar{w}^*\sin\psi + 2\bar{Z}^*\alpha_c^*\sin\psi \\ &+ \alpha_s^{**}\bar{x}\beta_{pc}\cos\psi + \alpha_s^{**}\bar{w}\cos\psi - \alpha_s^{*2}\bar{x}\sin\psi\cos\psi + 2\alpha_s^*\bar{w}^*\cos\psi - 2\bar{Z}^*\alpha_s^*\cos\psi \\ &+ \alpha_s^*\alpha_c^*\bar{x}(\cos^2\psi - \sin^2\psi) - 2\beta_{pc}\bar{w}^* + \bar{X}^{**}\sin\psi + \bar{Y}^{**}\cos\psi \\ &= L_v \end{aligned} \quad (46)$$

2.3 AERODYNAMIC FORCES

In deriving the aerodynamic forces, the following assumptions are made

1. Linear, quasi-steady aerodynamics
2. Blade stall, compressibility and reversed flow are neglected.
3. Uniform induced flow

Figure 4 shows the free airflow passing through the helicopter. And, Figure 5 shows the blade element geometry. The total velocity with respect to air mass in forward flight will be

$$\vec{U}_T = \vec{U}_{air} - \vec{U} \tag{47}$$

where,

$$\vec{U}_{air} = v_\infty \vec{I} - (V + v)\vec{K} \tag{48}$$

and $\vec{U}$ is the velocity obtained in Equation (21). Using the transformation $[T_R]$ and $[T_d]$ in Equations (2) and (4), We obtain the required velocity components in deformed coordinate with dimensionless form as follows:

$$\begin{aligned} U_{y'} = & -\theta\bar{w}^+\mu\cos\psi - \bar{v}^+\mu\cos\psi - \mu\sin\psi - \bar{v}^* - barx - \bar{u} \\ & - \alpha_s^*\bar{w}\cos\psi + \alpha_c^*\bar{w}\sin\psi + \bar{w}\beta_{pc} - \alpha_s^*\bar{x}\beta_{pc}\cos\psi \\ & + \alpha_c^*\beta_{pc}\bar{x}\sin\psi - \bar{X}^*\sin\psi - \bar{Y}^*\cos\psi - \theta\lambda \\ & - \theta\beta_{pc}\mu\cos\psi + \theta\alpha_c\mu - \theta\bar{w}^* + \theta\alpha_s{}^*\bar{x}\sin\psi \\ & + \theta\alpha_c^*\bar{x}\cos\psi + \theta\bar{Z}^* - \lambda\alpha_c\sin\psi + \lambda\alpha_s\cos\psi \end{aligned} \tag{49}$$

$$\begin{aligned} U_{z'} = & -\bar{w}^+\mu\cos\psi - \bar{w}^+\bar{X}^*\cos\psi + \bar{w}^+\bar{Y}^*\sin\psi - \lambda \\ & + \theta\mu\sin\psi + \theta\bar{x} + \bar{X}^*\theta\sin\psi + \bar{Y}^*\theta\cos\psi \\ & - \mu\beta_{pc}\cos\psi + \mu\alpha_c - \bar{w}^* + \alpha_s^*\bar{x}\sin\psi \\ & + \alpha_c^*\bar{x}\cos\psi - \bar{X}^*\beta_{pc}\cos\psi + \bar{Y}^*\beta_{pc}\sin\psi + \bar{Z}^* \end{aligned} \tag{50}$$

In the deformed coordinate, the dimensionless aerodynamic forces can be expressed as

$$F_{z'} = 0 \tag{51}$$

$$F_{y'} = \frac{\gamma}{6}[U_{z'}^2 - \frac{C_{d_s}}{a}U_{y'}^2] \tag{52}$$

$$F_{z'} = -\frac{\gamma}{6}[U_{z'}U_{y'}] \tag{53}$$

Then, we can transfer the aerodynamic forces above to undeformed rotating coordinates, which are

$$\begin{pmatrix} F_x \\ F_y \\ F_z \end{pmatrix} = [T_d]^T \begin{pmatrix} F_{x'} \\ F_{y'} \\ F_{z'} \end{pmatrix} \tag{54}$$

Then, the external aerodynamic forces are

$$L_w = F_z \tag{55}$$

$$L_v = F_y \tag{56}$$

2.4 FINAL EQUATIONS

Combining Equation (45), (46) and Equation (55), (56), we obtain the complete flapping and lead-lag equations as follows:

FLAPPING EQUATION

$$\begin{aligned}
&\Lambda_1^2\bar{w}^{++++} + (\Lambda_2^2 - \Lambda_1^2)R_e\theta\bar{v}^{++++} - \tau^+\bar{w}^+ - \tau\bar{w}^{++} + \bar{w}^{**} - 2\bar{v}^{*+} - \alpha_o^{**}\bar{x}\sin\psi \\
&- 2\alpha_o^*\bar{x}\cos\psi - \alpha_c^{**}\bar{x}\cos\psi + 2\alpha_c^*\bar{x}\sin\psi + \bar{X}^{**}\beta_{pc}\cos\psi - \bar{Y}^{**}\beta_{pc}\sin\psi - \bar{Z}^{**} + \beta_{pc}\bar{x} \\
&= \frac{\gamma}{6}\Big\{\theta\mu^2\sin^2\psi + \theta\bar{x}^2 + 2\theta\mu\bar{x}\sin\psi + \mu^2\alpha_c\sin\psi + \mu\alpha_o^*\bar{x}\sin^2\psi + \mu\alpha_c^*\bar{x}\sin\psi\cos\psi \\
&\quad + \mu\bar{Z}^*\sin\psi + \mu\alpha_c\bar{x} - \bar{w}^*\bar{x} + \alpha_o^*\bar{x}^2\sin\psi + \alpha_c^*\bar{x}^2\cos\psi - \bar{w}^+\mu^2\sin\psi\cos\psi + \bar{z}^*\bar{x} \\
&\quad - \mu\lambda\sin\psi - \lambda\bar{x} - \mu^2\beta_{pc}\sin\psi\cos\psi - \mu\bar{w}^*\sin\psi - \bar{w}^+\bar{x}\cos\psi - \mu\beta_{pc}\bar{x}\cos\psi\Big\}
\end{aligned} \tag{57}$$

LEAD-LAG EQUATION

$$\begin{aligned}
&\Lambda_2^2\bar{v}^{++++} + (\Lambda_2^2 - \Lambda_1^2)R_e\theta\bar{w}^{++++} - \tau^+\bar{v}^+ - \tau\bar{v}^{++} - \bar{v} \\
&- 2\int_0^{\bar{x}} \bar{w}^+\bar{w}^{*+}\,d\bar{x} + \bar{v}^{**} - \alpha_c^{**}\beta_{pc}\sin\psi - \alpha_c^{**}\bar{x}\bar{w}\sin\psi \\
&+ \alpha_c^{*2}\bar{x}\sin\psi\cos\psi - 2\alpha_c^*\bar{w}^*\sin\psi + 2\bar{Z}^*\alpha_c^*\sin\psi + \alpha_o^{**}\bar{x}\beta_{pc}\cos\psi \\
&+ \alpha_o^{**}\bar{w}\cos\psi - \alpha_o^{*2}\bar{x}\sin\psi\cos\psi + 2\alpha_o^*\bar{w}^*\cos\psi - 2\bar{Z}^*\alpha_o^*\cos\psi \\
&+ \alpha_o^*\alpha_c^*\bar{x}(\cos^2\psi - \sin^2\psi) - 2\beta_{pc}\bar{w}^* + \bar{X}^{**}\sin\psi + \bar{Y}^{**}\cos\psi
\end{aligned}$$

$$= \frac{\gamma}{6}\Big\{\bar{w}^{+2}\mu^2\cos^2\psi + \lambda^2 + \mu^2\beta_{pc}{}^2\cos^2\psi + \mu^2\alpha_c^2$$

$$+ \bar{w}^{*2} + \bar{Z}^{*2} + \alpha_a^{*2}\bar{x}^2\sin^2\psi + \alpha_c^{*2}\bar{x}^2\cos^2\psi$$

$$- \bar{w}^{+}\theta\mu^2\cos\psi\sin\psi - \bar{w}^{+}\theta\mu\bar{x}\cos\psi + 2\lambda\bar{w}^{+}\mu\cos\psi$$

$$+ 2\bar{w}^{+}\mu^2\beta_{pc}\cos\psi - 2\bar{w}^{+}\mu^2\alpha_c\cos\psi + 2\bar{w}^{+}\bar{w}^{*}\mu\cos\psi$$

$$- 2\bar{w}^{+}\alpha_a^{*}\mu\bar{x}\cos\psi\sin\psi - 2\bar{w}^{+}\alpha_c^{*}\mu\bar{x}\cos^2\psi - 2\bar{w}^{+}\bar{Z}^{*}\mu\cos\psi$$

$$- \theta\lambda\mu\sin\psi - \theta\mu^2\beta_{pc}\sin\psi\cos\psi + \theta\mu^2\alpha_c\sin\psi$$

$$- \bar{w}^{*}\theta\mu\sin\psi + \theta\alpha_a^{*}\mu\bar{x}\sin^2\psi + \theta\alpha_c^{*}\mu\bar{x}\sin\psi\cos\psi$$

$$+ \theta\bar{Z}^{*}\mu\sin\psi - \theta\lambda\bar{x} - \theta\mu\beta_{pc}\bar{x}\cos\psi + \theta\mu\alpha_c\bar{x} - \theta\bar{w}^{*}\bar{x}$$

$$+ \theta\bar{Z}^{*}\bar{x} + \theta\alpha_a^{*}\bar{x}^2\sin\psi + \theta\alpha_c^{*}\bar{x}^2\cos\psi + 2\lambda\mu\beta_{pc}\cos\psi$$

$$- 2\lambda\mu\alpha_c + 2\lambda\bar{w}^{*} - 2\lambda\alpha_a^{*}\bar{x}\sin\psi - 2\lambda\alpha_c^{*}\bar{x}\cos\psi - 2\lambda\bar{Z}^{*}$$

$$- 2\mu^2\beta_{pc}\alpha_c\cos\psi + 2\bar{w}^{*}\mu\beta_{pc}\cos\psi - 2\alpha_a^{*}\beta_{pc}\mu\bar{x}\sin\psi\cos\psi$$

$$- 2\alpha_c^{*}\beta_{pc}\mu\bar{x}\cos^2\psi - 2\bar{z}^{*}\mu\beta_{pc}\cos\psi - 2\bar{w}^{*}\mu\alpha_c + 2\alpha_c\alpha_a^{*}\bar{x}\sin\psi$$

$$+ 2\alpha_c^{*}\alpha_a\mu\bar{x}\cos\psi + 2\bar{Z}^{*}\mu\alpha_c - 2\bar{w}^{*}\alpha_a^{*}\bar{x}\sin\psi - 2\bar{w}^{*}\alpha_c^{*}\bar{x}\cos\psi$$

$$- 2\bar{Z}^{*}\bar{w}^{*} + 2\alpha_a^{*}\alpha_c^{*}\bar{x}^2\sin\psi\cos\psi + 2\bar{Z}^{*}\alpha_a^{*}\bar{x}\sin\psi + 2\bar{Z}^{*}\alpha_c^{*}\bar{x}\cos\psi$$

$$- \frac{C_{d_e}}{a}[\bar{x}^2 + \mu^2\sin^2 + 2\mu\bar{x}\sin\psi + 2\mu\bar{x}^{*}\sin^2\psi$$

$$+ 2\bar{x}\bar{X}^{*}\sin\psi + 2\mu\bar{Y}^{*}\sin\psi\cos\psi + 2\bar{x}\bar{Y}^{*}\cos\psi]\Big\} \qquad (58)$$

THE BOUNDARY CONDITION

$$V_{x'}\delta u\Big|_0^R + \{V_{x'}v' - [M_{z'} + My'R_e\theta]'\}\delta v\Big|_0^R + [M_{z'} + M_{y'}R_e\theta]\delta v'\Big|_0^R$$

$$+ \{V_{x'}w - [M_{z'}R_e\theta - M_{y'}]'\}\delta w\Big|_0^R + [M_{z'}R_e\theta - M_{y'}]\delta w'\Big|_0^R$$

$$- me\cos\theta[\ddot{\bar{Y}}\sin\Omega t - \ddot{\bar{X}}\cos\Omega t - \Omega^2 x - 2\Omega\dot{v}]\delta v\Big|_0^R$$

$$- me\sin\theta[\ddot{\bar{Y}}\sin\Omega t - \ddot{\bar{X}}\cos\Omega t - \Omega^2 x - 2\Omega\dot{v}]\delta w\Big|_0^R$$

$$= 0 \qquad (59)$$

It may be noted that for a rigid blade (for which $w = \beta x$ and $v = \varsigma x$, the flapping Equation (57) and the lead-lag Equation (58) reduce to those of Reference 13 with the exception of nonlinear higher-order terms.

3. HUB LOAD EQUATIONS

The hub loads including the shears and moments, in both rotating and fixed coordinate systems, are shown in Figure 6. C_x, C_y, and C_z are radial, lead-lag, and flap shear components; and C_u, C_v, C_w are torsional, in-plane and out-of-plane moment components in the rotating coordinate system. C_Z, C_X, and C_Y are the vertical thrust, forward drag, and side force components in the fixed coordinate system. The loads with respect to the rotating system are called rotating loads and those corresponding to the fixed system are called nonrotating loads. They are derived in detail below.

3.1 ROTATING LOADS

The expressions for the root shear and moment components in the rotating coordinate system are formed by spanwise integration of the aerodynamic and inertia loads as follows:

$$C_x = \frac{3}{\gamma}\int_0^1 \bar{F}_x \, d\bar{X} - \frac{3}{\gamma}\int_0^1 \bar{a}_{ox} \, d\bar{x} \tag{60}$$

$$C_y = \frac{3}{\gamma}\int_0^1 \bar{F}_y \, d\bar{x} - \frac{3}{\gamma}\int_0^1 \bar{a}_{oy} d\bar{x} \tag{61}$$

$$C_z = \frac{3}{\gamma}\int_0^1 \bar{F}_z \, d\bar{x} - \frac{3}{\gamma}\int_0^1 \bar{a}_{oz} \, d\bar{x} \tag{62}$$

$$C_w = \frac{3}{\gamma}\int_0^1 \bar{F}_z \bar{x} \, d\bar{x} + \frac{3}{\gamma}\int_0^1 \bar{a}_{oz} \bar{x} \, d\bar{x} + \frac{3}{\gamma}\int_0^1 \bar{F}_x \bar{w} \, d\bar{x} - \frac{3}{\gamma}\int_0^1 \bar{a}_{ox} \bar{w} \, d\bar{x} \tag{63}$$

$$C_u \approx 0 \tag{64}$$

$$C_v \approx 0 \tag{65}$$

where the aerodynamic forces are obtained in Equation (54), and the dimentionless accelerations are as follows:

$$\begin{aligned} \bar{a}_{ox} = {} & \bar{u}^{**} - 2\alpha_s^* \bar{w}^* \sin\psi + 2\alpha_c^* \bar{w}^* \cos\psi - 2\bar{v}^* - \alpha_s^{*2} \bar{x} \sin^2\psi \\ & - \alpha_c^{*2} \bar{x} \cos\psi + 2\alpha_s^* \alpha_c^* \bar{x} \sin\psi \cos\psi - 2\alpha_s^* \beta_{pc} \bar{x} \cos\psi \\ & + 2\alpha_c^* \beta_{pc} \bar{x} \sin\psi - \bar{x} - \bar{u} + \beta_{pc} \bar{w} - \alpha_s^{**} \bar{w} \cos\psi \end{aligned}$$

$$+ \alpha_c^{\bullet\bullet}\bar{w}\cos\psi + \bar{X}^{\bullet\bullet}\cos\psi + \bar{Y}^{\bullet\bullet}\sin\psi \tag{66}$$

$$\begin{aligned} a_{oy} = {} & \bar{v}^{\bullet\bullet} + 2\bar{u}^{\bullet} - 2\alpha_s^{\bullet}\bar{w}^{\bullet}\cos\psi - 2\alpha_c^{\bullet}\bar{w}^{\bullet}\sin\psi - 2\beta_{pc}\bar{w}^{\bullet} \\ & - \alpha_s^{\bullet}\bar{w}\sin\psi + \alpha_c^{\bullet}\bar{w}\cos\psi - \bar{v} - \alpha_s^{\bullet 2}\bar{x}\sin\psi\cos\psi \\ & - \alpha_c^{\bullet}\alpha_s^{\bullet}\bar{x}\sin^2\psi + \alpha_s^{\bullet}\alpha_c^{\bullet}\bar{x}\cos^2\psi + \alpha_s^{\bullet}\beta_{pc}\bar{x}\sin\psi \\ & + \alpha_c^{\bullet 2}\bar{x}\sin\psi\cos\psi + \alpha_s^{\bullet\bullet}\beta_{pc}\bar{x}\cos\psi - \alpha_c^{\bullet\bullet}\beta_{pc}\bar{x}\sin\psi \\ & - \alpha_s^{\bullet\bullet}\bar{w}\cos\psi + \alpha_s^{\bullet}\bar{w}\sin\psi - \alpha_c^{\bullet\bullet}\bar{w}\sin\psi - \alpha_c^{\bullet}\bar{w}\cos\psi \\ & - \bar{X}^{\bullet\bullet}\sin\psi + \bar{Y}^{\bullet\bullet}\cos\psi \end{aligned} \tag{67}$$

$$\begin{aligned} a_{oz} = {} & \bar{w}^{\bullet\bullet} + 2\alpha_s^{\bullet}\bar{x}\cos\psi + 2\alpha_c^{\bullet}\bar{x}\sin\psi + \beta_{pc}\bar{x} \\ & + \alpha_s^{\bullet\bullet}\bar{x}\sin\psi - \alpha_c^{\bullet\bullet}\bar{x}\cos\psi + \bar{Z}^{\bullet\bullet} \end{aligned} \tag{68}$$

3.2 NON-ROTATING LOADS

The shear and moment components in the fixed coordinate system are formed from the load components in the rotating coordinate system. They can be simply expressed as

$$C_X = C_x\cos\psi - C_y\sin\psi \tag{69}$$

$$C_Y = C_x\sin\psi + C_y\cos\psi \tag{70}$$

$$C_Z = C_z \tag{71}$$

$$C_L = -C_w\sin\psi \tag{72}$$

$$C_M = C_w\cos\psi \tag{73}$$

They can be put into matrix form as done in Reference 13. It is:

$$\begin{pmatrix} C_M \\ C_L \\ C_X \\ C_Y \\ C_Z \end{pmatrix} = \left[\Phi(\psi)\right] \begin{pmatrix} \theta_o \\ \theta_s \\ \theta_c \\ \lambda \\ \beta \\ \beta_{pc} \\ \frac{C_{d_o}}{a} \\ \alpha_c \end{pmatrix} + \left[A(\psi)\right] \begin{pmatrix} \alpha_c \\ \alpha_s \\ \bar{X} \\ \bar{Y} \\ \bar{Z} \end{pmatrix} + \left[B(\psi)\right] \begin{pmatrix} \alpha_c^{\bullet} \\ \alpha_s^{\bullet} \\ \bar{X}^{\bullet} \\ \bar{Y}^{\bullet} \\ \bar{Z}^{\bullet} \end{pmatrix} + \left[D(\psi)\right] \begin{pmatrix} \alpha_c^{\bullet\bullet} \\ \alpha_s^{\bullet\bullet} \\ \bar{X}^{\bullet\bullet} \\ \bar{Y}^{\bullet\bullet} \\ \bar{Z}^{\bullet\bullet} \end{pmatrix}$$

$$+ \left\{\vec{F}\left(\bar{w}, \bar{w}^{+}, \bar{w}^{\bullet}, \bar{w}^{\bullet+}, \bar{w}^{\bullet\bullet}, \bar{w}^{\bullet++}, \bar{w}^{\bullet\bullet+}, \bar{v}, \bar{v}^{\bullet}, \bar{v}^{\bullet\bullet}\right)\right\} \tag{74}$$

Again, Equation (74) matches the similar equation in Reference 13 very well, except for the additional nonlinear terms.

4.FUSELAGE EQUATIONS

In this research, the same model as in Reference 13 is used for fuselage, except that X and Y axes have opposite positive directions. Figure 7 shows the fuselage model in the longitudinal and pitch directions.

This model includes 9 degrees of freedom. These are:

1) vertical rigid-body;

2) rigid-body pitch;

3) rigid-body roll;

4) rigid lateral;

5) rigid longitudinal;

6) elastic vertical;

7) elastic lateral;

8) elastic pylon in pitch;

9) elastic pylon in roll.

The model also includes vertical offsets between the fuselage center of mass, the pylon focus, the pylon center of mass, and the rotor center.

The fuselage is modeled as a uniform beam with a lumped mass M_c added at the center. The mass of the pylon is separated from the fuselage, which is connected to the fuselage through pitch and roll torsional springs. The fuselage equations of motion are the same as those in Reference 13, except that the X and Y axes are reversed.

5. SOLUTION METHOD

5.1 GALERKIN METHOD

The flap-lag equations of motion, Equation (57) and (58), are nonlinear, variable coefficient, integro-partial differential equations. First, these equations can be reduced to nonlinear ordinary differential equations in terms of the generalized coordinates by use of the modal form $w = \phi_j q_j$ and $v = \phi_l p_l$, and the Galerkin method as below:

$$\begin{pmatrix} M_{ij} & M_{il} \\ M_{kj} & M_{kl} \end{pmatrix} \begin{pmatrix} \ddot{q}_j \\ \ddot{p}_l \end{pmatrix} + \begin{pmatrix} C_{ij} & C_{il} \\ C_{kj} & C_{kl} \end{pmatrix} \begin{pmatrix} \dot{q}_j \\ \dot{p}_l \end{pmatrix} + \begin{pmatrix} K_{ij} & K_{il} \\ K_{kj} & K_{kl} \end{pmatrix} \begin{pmatrix} q_j \\ p_l \end{pmatrix} = \begin{pmatrix} F_i \\ F_k \end{pmatrix} \tag{75}$$

Where M, C, and K are functions of q, p, and their derivatives and where

$i, j = 1, \ldots$ m number of flap degrees of freedom;

and

$k, l = 1, \ldots$ n number of lead-lag degrees of freedom.

5.2 HARMONIC BALANCE

As done in Reference 13, fuselage equations can be transformed into a set of linear, algebraic equations by a harmonic balance which is formulated in matrix notation for a linear, multi-degree-of-freedom system in Reference 7. In our case, the equations are nonlinear. Therefore, an important conclusion obtained in Reference 13 can be used. As mentioned before, it says that the addition of inplane degrees of freedom does not significantly affect the plunge vibrations for the cases considered, and these cases are for resonable configurations. Figure 8 and 9 shows the comparison of plunge vibration with or without inplane degrees of freedom.

Therefore, we can first solve the plunge-pitch-roll problem with inplane parameters eliminated. To do this, the flapping equation is expressed as below:

$$\begin{pmatrix} M_{11} & \cdots & M_{1i} \\ \vdots & \ddots & \vdots \\ M_{i1} & \cdots & M_{ij} \end{pmatrix} \begin{pmatrix} q_1^{\bullet\bullet} \\ \vdots \\ q_j^{\bullet\bullet} \end{pmatrix} + \begin{pmatrix} C_{11} & \cdots & C_{1i} \\ \vdots & \ddots & \vdots \\ C_{i1} & \cdots & C_{ij} \end{pmatrix} \begin{pmatrix} q_1^{\bullet} \\ \vdots \\ q_j^{\bullet} \end{pmatrix} + \begin{pmatrix} K_{11} & \cdots & K_{1i} \\ \vdots & \ddots & \vdots \\ K_{i1} & \cdots & K_{ij} \end{pmatrix} \begin{pmatrix} q_1 \\ \vdots \\ q_j \end{pmatrix}$$

$$= \left[\bar{Q}(\psi)\right] \begin{pmatrix} \theta_o \\ \theta_s \\ \theta_c \\ \lambda \\ \beta \\ \beta_{pc} \\ \frac{C_{d_o}}{a} \\ \bar{\alpha}_c \end{pmatrix} + \left[\bar{A}(\psi)\right] \begin{pmatrix} \alpha_c \\ \alpha_s \\ \bar{Z} \end{pmatrix} + \left[\bar{B}(\psi)\right] \begin{pmatrix} \alpha_c^* \\ \alpha_s^* \\ \bar{Z}^* \end{pmatrix} + \left[\bar{D}(\psi)\right] \begin{pmatrix} \alpha_c^{**} \\ \alpha_s^{**} \\ \bar{Z}^{**} \end{pmatrix} \tag{76}$$

and the load equation (74) becomes

$$\begin{pmatrix} \tilde{C}_M \\ \tilde{C}_L \\ \tilde{C}_Z \end{pmatrix} = \left[\tilde{\Phi}(\psi)\right] \begin{pmatrix} \theta_o \\ \theta_s \\ \theta_c \\ \lambda \\ \beta \\ \beta_{pc} \\ \frac{C_{d_o}}{a} \\ \bar{\alpha}_c \end{pmatrix} + \left[\tilde{A}(\psi)\right] \begin{pmatrix} \alpha_c \\ \alpha_s \\ \bar{Z} \end{pmatrix} + \left[\tilde{B}(\psi)\right] \begin{pmatrix} \alpha_c^* \\ \alpha_s^* \\ \bar{Z}^* \end{pmatrix} + \left[\tilde{D}(\psi)\right] \begin{pmatrix} \alpha_c^{**} \\ \alpha_s^{**} \\ \bar{Z}^{**} \end{pmatrix}$$

$$+ \left[\tilde{E}(\psi)\right] \begin{pmatrix} q_1 \\ \vdots \\ q_j \end{pmatrix} + \left[\tilde{F}(\psi)\right] \begin{pmatrix} q_1^* \\ \vdots \\ q_j^* \end{pmatrix} + \left[\tilde{G}(\psi)\right] \begin{pmatrix} q_1^{**} \\ \vdots \\ q_j^{**} \end{pmatrix} \tag{77}$$

For the fuselage equations, we have eliminated $\bar{X}$, $\bar{Y}$, and $\bar{Y}_F$, and their derivatives. Now, these equations are linear ordinary differential equations with peoriodic coefficients. They are easily solved by harmonic balance technique and impedance matching. The control vector components θ_o, θ_s, θ_c, λ, β, β_{pc}, $\frac{C_{d_o}}{a}$, and $\bar{\alpha}_c$ can be

obtained from a trim procedure.

For the next step, we go to Equation (75) with $q_1 \ldots q_j$ and α_c, α_s, and $\bar{Z}$ and their derivitives as knowns. The flap-lag Equations (75) can be further expressed as

$$\begin{pmatrix} M_{ij} & M_{il} \\ M_{kj} & M_{kl} \end{pmatrix} \begin{pmatrix} \ddot{q}_j \\ \ddot{p}_l \end{pmatrix} + \begin{pmatrix} C_{ij} & C_{il} \\ C_{kj} & C_{kl} \end{pmatrix} \begin{pmatrix} \dot{q}_j \\ \dot{p}_l \end{pmatrix} + \begin{pmatrix} K_{ij} & K_{il} \\ K_{kj} & K_{kl} \end{pmatrix} \begin{pmatrix} q_j \\ p_l \end{pmatrix}$$

$$= \left[\hat{Q}(\psi)\right] \begin{pmatrix} \theta_o \\ \theta_s \\ \theta_c \\ \lambda \\ \beta \\ \beta_{pc} \\ \frac{C_{d_o}}{a} \\ \bar{\alpha}_c \end{pmatrix} + \left[\hat{A}(\psi)\right] \begin{pmatrix} \alpha_c \\ \alpha_s \\ \bar{X} \\ \bar{Y} \\ \bar{Z} \end{pmatrix} + \left[\hat{B}(\psi)\right] \begin{pmatrix} \alpha_c^* \\ \alpha_s^* \\ \bar{X}^* \\ \bar{Y}^* \\ \bar{Z}^* \end{pmatrix} + \left[\hat{D}(\psi)\right] \begin{pmatrix} \alpha_c^{**} \\ \alpha_s^{**} \\ \bar{X}^{**} \\ \bar{Y}^{**} \\ \bar{Z}^{**} \end{pmatrix} \tag{78}$$

and the load Equations (74) can be further expressed as

$$\begin{pmatrix} C_M \\ C_L \\ C_X \\ C_Y \\ C_Z \end{pmatrix} = \left[\Phi(\psi)\right] \begin{pmatrix} \theta_o \\ \theta_s \\ \theta_c \\ \lambda \\ \beta \\ \beta_{pc} \\ \frac{C_{d_o}}{a} \\ \bar{\alpha}_c \end{pmatrix} + \left[A(\psi)\right] \begin{pmatrix} \alpha_c \\ \alpha_s \\ \bar{X} \\ \bar{Y} \\ \bar{Z} \end{pmatrix} + \left[B(\psi)\right] \begin{pmatrix} \alpha_c^* \\ \alpha_s^* \\ \bar{X}^* \\ \bar{Y}^* \\ \bar{Z}^* \end{pmatrix} + \left[D(\psi)\right] \begin{pmatrix} \alpha_c^{**} \\ \alpha_s^{**} \\ \bar{X}^{**} \\ \bar{Y}^{**} \\ \bar{Z}^{**} \end{pmatrix}$$

$$+ \left[E(\psi)\right] \begin{pmatrix} q_j \\ p_l \end{pmatrix} + \left[F(\psi)\right] \begin{pmatrix} q_j^* \\ p_l^* \end{pmatrix} + \left[G(\psi)\right] \begin{pmatrix} q_j^{**} \\ p_l^{**} \end{pmatrix} \tag{79}$$

Then, using flap-lag Equations (78), load Equations (79) and complete fuselage equations, we can finally solve the inplane problem.

6. STATEMENT OF WORK

In helicopter preliminary design stage, it is very important for designers to determine the helicopter structure dynamic parameters. Besides getting a stable system, we hope that helicopter vibrations can be reduced as much as possible in the helicopter flight envelope. Since different combinations of fuselage and rotor parameters can cause quite different vibration levels, we should study them carefully. As is well known, most hingeless rotors can be considered as relatively soft flapwise, except the ABC blade which is stiff flapwise. So, we will choose a soft flapwise rotor system as done in Reference 7 and Reference 13. For the inplane direction, soft inplane and stiff inplane both are common. Therefore, this investigation includes both soft inplane and stiff inplane rotors. In brief, we will change fuselage dynamic parameters (the fuselage first bending natural frequencies in vertical and lateral directions, and the pylon torsional natural frequencies in pitch and roll directions) to match two categories of rotor systems, which are soft flapwise, and both soft inplane and stiff inplane. Also, the fuselage layout will affect the dynamic response significantly, as obtained in Reference 13, the configurations without or with offsets are concerned.

In order to finally solve the Equations (78) and (79) with different dynamic parameters described above, the detailed procedure are as follows. At first, Equations (76) and (77) should be solved in order to obtain the generalized coordinates $q_1 \ldots q_j$ and α_c, α_s, and $\bar{Z}$ and their first and second derivatives as knowns. To do so, three nonrotating out-of-plane bending modes are used, which are the same as those in Reference 8. Also, the baseline parameters are chosen as the same as those in Reference 8 for comparison purposes. The baseline parameters are as follows:

Rotor:	4 blades	$\gamma = 8$	$\mu = .3$
	$p = 1.12$	$\omega_2 = 2.5$	$\omega_3 = 4.5$
Fuselage	$\bar{r}_{gm} = .37$	$\bar{r}_{gL} = .14$	
	$\bar{\omega}_{fv} = 1.53$	$\bar{\omega}_{fm} = 2.58$	$\bar{\omega}_{fL} = 1.18\bar{\omega}_{fm}$
	$\bar{\omega}_{fv}/\bar{\omega}_{cv} = 1.45$	$\bar{\omega}_{fm}/\bar{\omega}_{cm} = 10.0$	$\bar{\omega}_{fL}/\bar{\omega}_{cL} = 4.47$
	$g_v = g_m = g_L = .02$	$h = d_F = d_p = 0.0$	
Trim Condition:	$\lvert\bar{C}_Z\rvert = .0144$	$\lvert\bar{C}_L\rvert = \lvert\bar{C}_M\rvert = 0.0$	
	$\alpha_c = -.0715$	$\lambda = .03187$	

Next, we add three nonrotating blade inplane bending modes. In order to study the dynamic response for both soft-inplane and stiff-inplane rotors, two sets of three nonrotating blade inplane bending modes are used to correspond to different rotors. For the comparison purposes, the first inplane nonrotating bending frequencies corresponding to soft inplane and stiff inplane rotors are the same as those in Reference 13, which are $\omega_\zeta = .7$ and $\omega_\zeta = 1.4$, respectively. Also, we need both lateral damping coeffecients of the fuselage and the steady portion of side forces, which are $g_y = .02, .002$, and $|\bar{C}_X| = |\bar{C}_Y| = 0.0$, the same as those in Reference 13.

The last step is to study the effects of offsets. The same parameters, $h = .4$, $d_p = 0.0$, and $d_F = .2$ as those in Reference 13, are used for both soft inplane and stiff inplane cases. Thus, we can obtain all responses for different possible situations.

At the present point in our research we are transfering our computer codes from the VAX system at Washington University to the CDC system at Georgia Institute of Technology. When this work is completed, we will be able to continue the numerical work and should have our first answer shortly. The first runs will be validation runs to ensure that we can repeat the results of References 8, 12, and 13. Then we will procede to studies of parameter variations.

7. NOMENCLATURE

a	= slope of lift curve, 1/rad
A	= ratio of rotor mass to moment of inertia, $M\bar{x}R/I_y$
b	= number of blades
C_{d_o}	= blade profile drag coefficient
$\hat{C}_Z$	= conventional thrust coefficient, thrust$/\rho\pi\Omega^2R^4$
C_X, C_Y, C_Z, C_M, C_L	= vibratory portion of nondimensional longitudinal force, lateral force, thrust, pitch and roll moment over σa
$\bar{C}_X, \bar{C}_Y, \bar{C}_Z, \bar{C}_M, \bar{C}_L$	= steady portion of coefficients
d_F	= offset between focus and center of pylon, divided by R
d_p	= offset between focus and center of pylon, divided by R
d_r	= offset between hub and center of pylon, divided by R
e	= mass centroid offset from elastic axis of a blade
EI	= beam cross-section bending stiffness
$\{\vec{F}\}$	= vector of forces
g	= nondimensional acceleration of gravity, g/Ω^2R
g_z, g_y, g_m, g_l	= plunge, lateral, pitch and roll structural damping, $\approx 2\zeta/\omega_n$
h	= offset between hub and focus, divided by R
$[H]$	= fuselage receptance
$[I]$	= identity matrix
I_{y_1}	= pitch inertia moment of pylon, divided by M_pR^2
I_{x_1}	= roll inertia moment of pylon, divided by M_pR^2
I_{y_2}	= pitch inertia moment of fuselage, divided by M_FR^2
I_{x_2}	= roll inertia moment of fuselage, divided by M_FR^2
l	= length of the beam, m

m	= mass per unit beam length, kg/m
M_c	= lumped mass on the center of fuselage, kg
M_p	= mass of pylon, kg
M_F	= mass of fuselage, $M_c + ml$, kg/m
M_f	= mass of whole fuselage, $M_c + ml + M_p$, kg
q_i	= generalized coordinates
$\bar{r}_{pm}, \bar{r}_{pl}$	= radius of gyration of pylon in pitch, roll, divided by R
$\bar{r}_{Fm}, \bar{r}_{FL}$	= radius of gyration of fuselage in pitch, roll, divided by R
R	= rotor radius, m
R_v	= beam mass divided by whole airframe mass, $ml/(ml + M_c + M_p)$
$[T_d]$	= transformation matrix, Equation (4)
$[T_R]$	= transformation matrix, Equation (2)
U	= blade airfoil velocity with respect to the air mass, m/sec also strain energy, N-m
U_p, U_T	= velocity components of blade airfoil section, perpendicular and parallel to the chord respectively, m/sec
u, v, w	= elastic deformation in x, y, z directions respectively, m
V	= velocity vector of a arbitrary point on deformed blade, m/sec
δW	= virtual work, N-m
x	= distance along fuselage, nose to tail, or distance along radius of rotor, root to tip, divided by R

x, y, z = rotating coordinates fixed on the blade

x', y', z' = deformed coordinates fixed on the blade

X, Y, Z = fixed fuselage coordinates

Y_F, Z_F = dimensionless fuselage elastic degree of freedom in vertical and lateral directions

α_c = pitch angle of hub, fuselage, positive nose up, rad

α_s = roll angle of hub, fuselage, positive advancing side up, rad

$\bar{\beta}$ = equilibrium flapping angle, rad
$\beta_o + \beta_s \sin\psi + \beta_c \cos\psi$

β_o = coning angle, rad

β_s = lateral cyclic flap angle, rad

β_c = longitudinal cyclic flap angle, rad

β_{pc} = pre-cone angle

γ = Lock number

δ = first variation

ϵ = scaling parameter, (=.1)

ς, η = blade cross-section principal axes coordinates

$\{\vec{\theta}\}$ = vector of control variables

$\bar{\theta}$ = equilibrium pitch angle,
$\theta_o + \theta_s \sin\psi + \theta_c \cos\psi + \theta_\beta(\bar{\theta} - \beta_{pc}) + \theta_\varsigma \bar{\varsigma}$

$\theta_o, \theta_s, \theta_c$ = collective and cyclic pitch, rad

λ = inflow ratio

μ = advance ratio

μ_p = ratio of mass of pylon to mass of fuselage, $M_p/(ml + M_c)$

μ_c = ratio of lumped mass to the uniformly distributed mass, M_p/ml

ρ = air density, kg/m^3

σ	= rotor solidity
σ_{ij}	= stress tensor components, N/m^2
τ	= dimensionless tenssion
ψ	= blade azimuth angle, nondimensional time
ω	= natural frequency of fuselage, divided by Ω
ω_{xy}	= frequency of "y" motion with "x" boundary condition, divided by Ω; y = z,y,m,L plunge, lateral, pitch, roll, x = c, f cantilevered,free
Ω	= rotor speed, rad/sec
$()^*$	= $d( )/d\psi$
$\dot{()}$	= $d( )/dt$
$()^+$	= $d( )/d\tilde{x}$
$()'$	= $d( )/dx$

8. REFERENCES

(1) Gestenberger, Walter and Wood, Edward R., "Analysis of Hilecopter Aeroelastic Characteristics in High-Speed Flight", AIAA Journal, Vol. 1, No. 10, October 1964.

(2) Staley, J. A. and Sciarra, J. J., "Coupled Rotor/Airframe Vibration Predication methods", Rotorcraft Dynamics, NASA SP-352, 1974.

(3) Hohenemser, Kurt H. and Yin, Sheng-Kuang, "The Role of Rotor Impedance in the Vibration Analysis of Rotorcraft", Fourth European Powered Lift Aircraft Forum, Stressa, Italy, September 1978.

(4) Kato, Kanichiro and Yamane, Takaski, "Calculation of Rotor Impedance for Hovering Articulated-Rotor Helicopters", AIAA Journal, Vol. 16, No. 1, January 1979.

(5) Kuczynski, W. A. and Sissingh, G. J., "Characteristics of Hingeless Rotors with Hub Moment Feedback Controls Including Experimental Rotor Frequency Response", NASA CR 114427, January 1972.

(6) Viswanthan, S. P. and Meyers, A. W., "Reduction of Helicopter Vibration through Control of Hub Impedance", Journal of the American Helicopter Society, Vol. 25, No. 4, October, 1980, pp. 5-12

(7) Peters, David A. and Ormiston, Robert A., "Flapping Response Characteristics of Hingeless Rotor Blades by a Generalized Harmonic Balance Method", NASA TN D-7856, February 1975.

(8) Hsu, T-K and Peters, David A., "Coupled Rotor/Airframe Vibration Analysis by a combined Harmonic-Balance, Impedance-Matching Method", Journal of American Hilecopter Society, Vol. 27, No. 1, January 1982, pp. 25-34

(9) Kuns, D., "Effects of Rotor-Body Coupling in a Linear Rotorcraft Vibration Modal", Proceedings of the 36th Annual Forum of the American Helicopter Society, Washington, DC, May 1980.

(10) Kuns, D., "A Nonlinear Response Analysis and Solution Method for Rotorcraft Vibration", Journal of the American Helicopter Society, Vol. 28, No. 1, January 1983.

(11) Schrage, Daniel P., "Effect of Structural Parameters on Elastic Flap-Lag Forced Response of a Rotor Blade in Forward Flight", Doctor of Science thesis, Washington University in St. Louis, May, 1978.

(12) Eipe, Abraham, "Effect of Some Structural Parameters on Elastic Rotor Loads by an Iterative Harmonic Balance", Doctor of Science Thesis, Washington University in St. Louis, December, 1979.

(13) Huang, Ming-Sheng, "Coupled Rotor-Airframe Vibrations with Elastic Fuselage and Inplane Degrees of Freedom", Master of Science Thesis, Washington University in St. Louis, June, 1983.

9. ACKNOWLEDGEMENT

The work was sponsored by the United States Army Research Office, Grant No. ARO-DAAG-29-80-C-0092. The view, opinions, and/or findings contained in this report are those of the authors and should not be construed as an official department of the Army position, policy, or decision, unless so designated by other documentation.

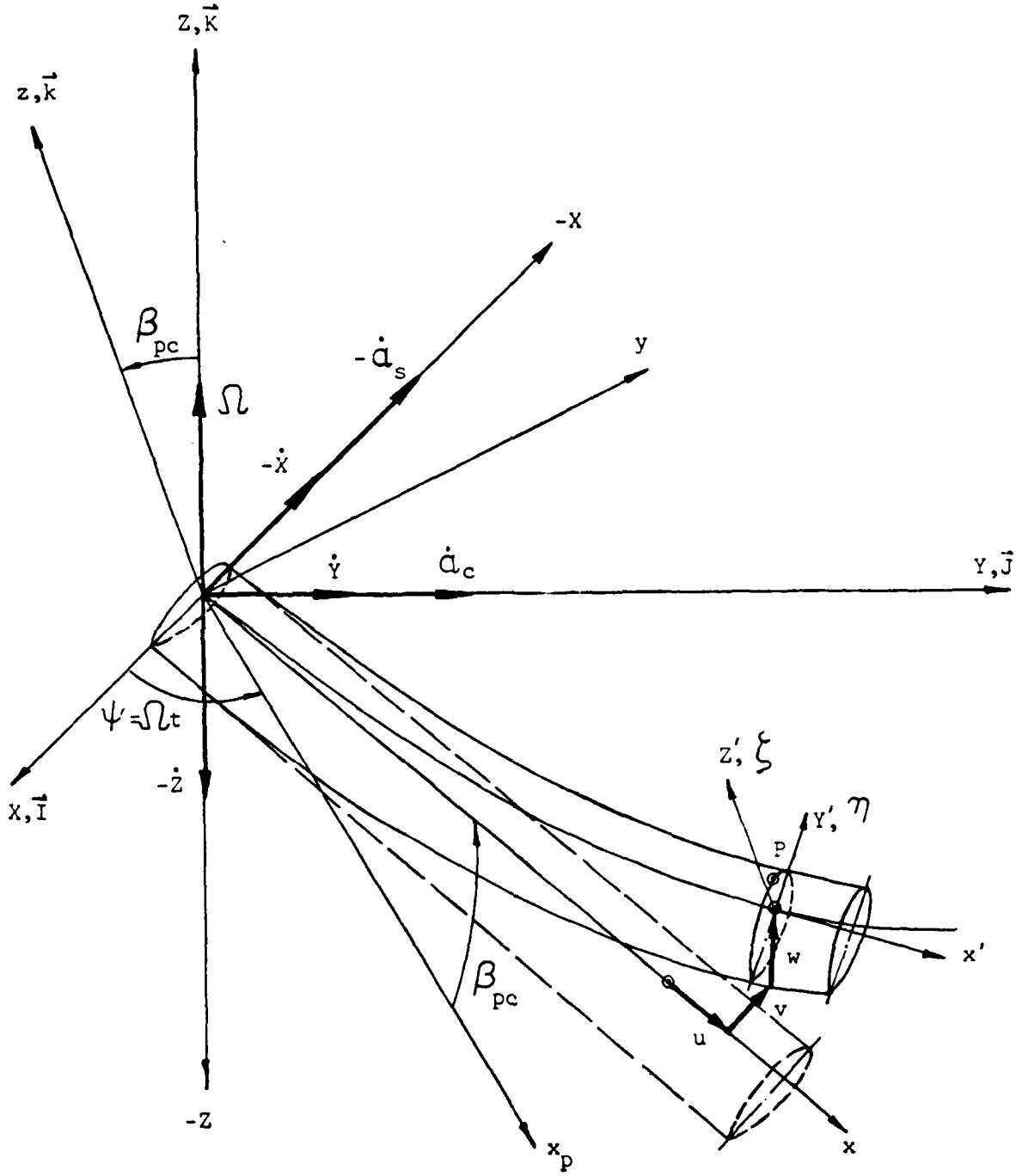

Figure 1 Fixed, rotating and deformed Coordinate systems of an elastic blade

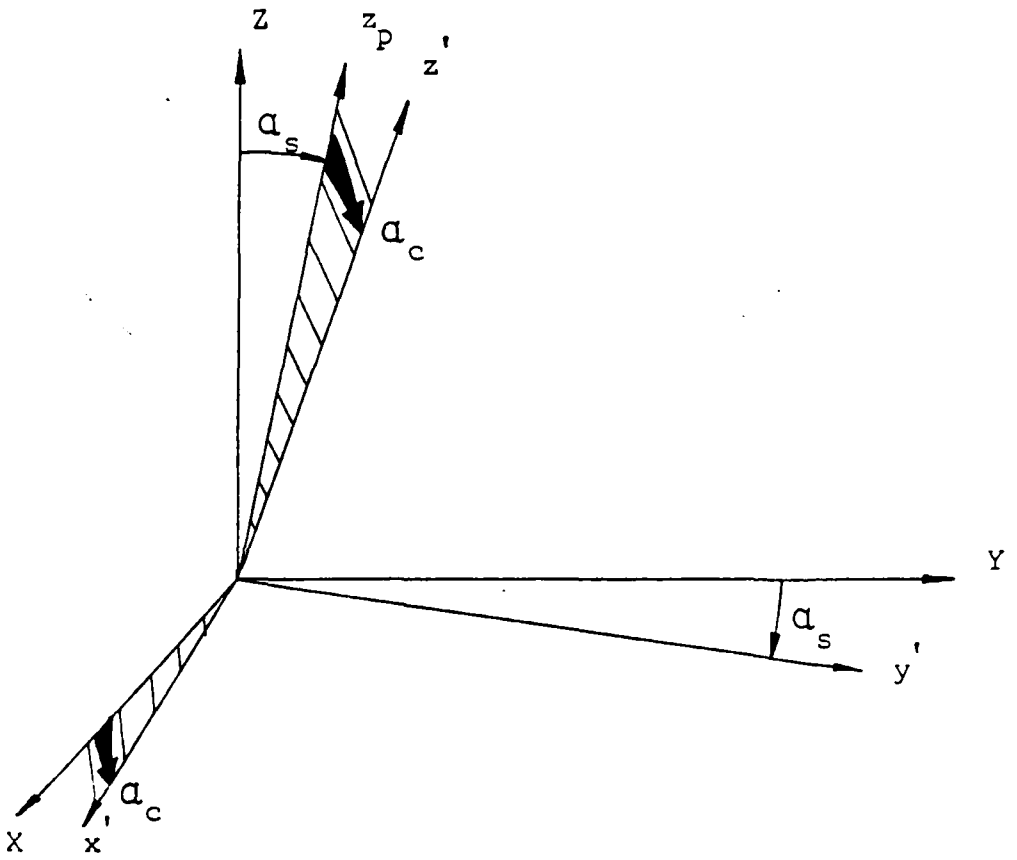

Figure 2 Considering pitching and rolling angles

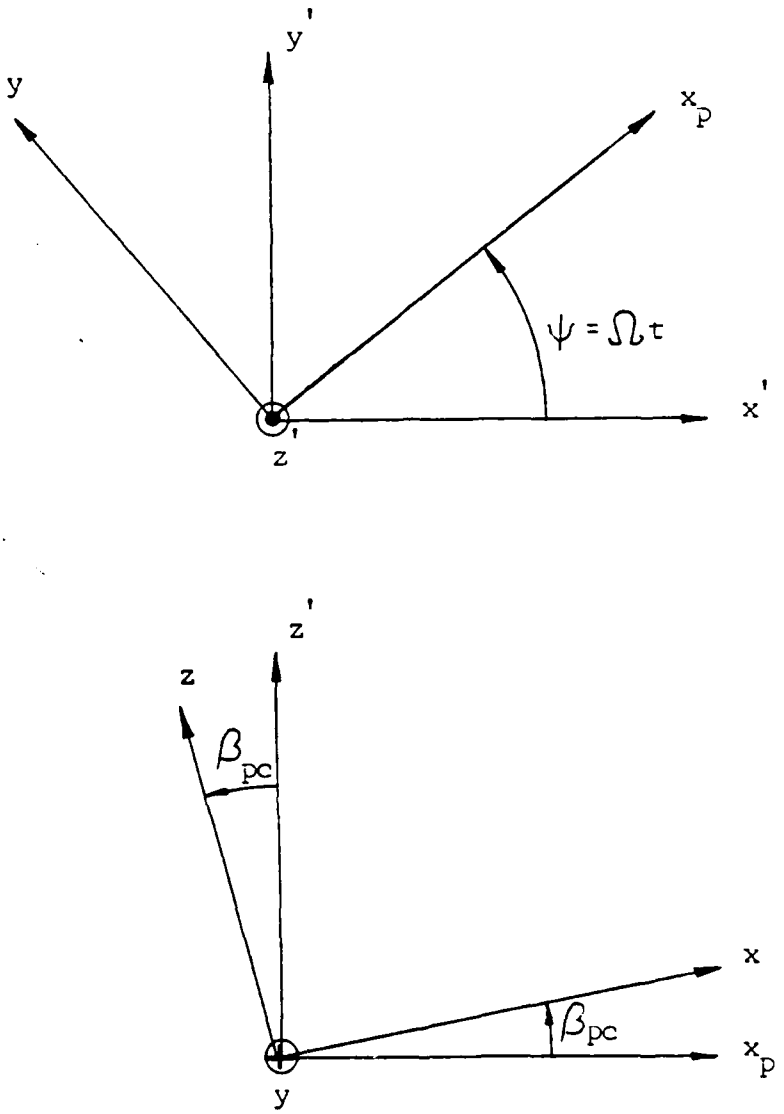

Figure 3 Considering azimuth and pre-cone angles

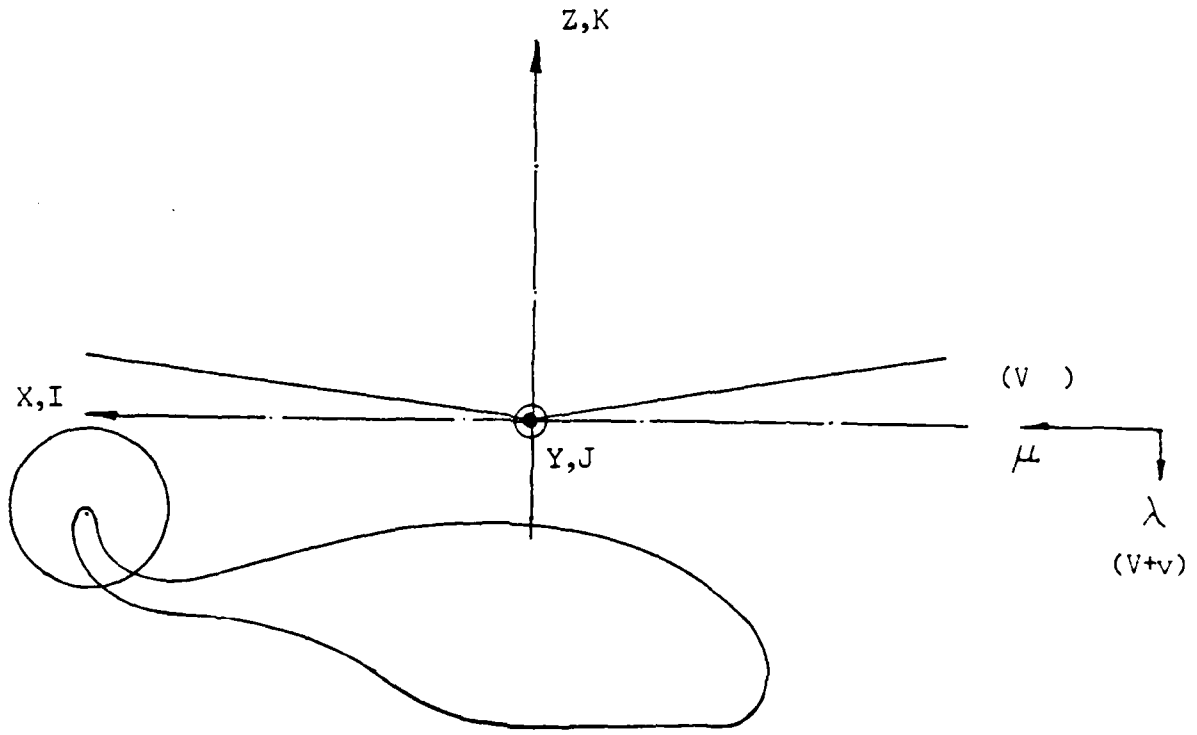

Figue 4 Free airflow passing through the helicopter

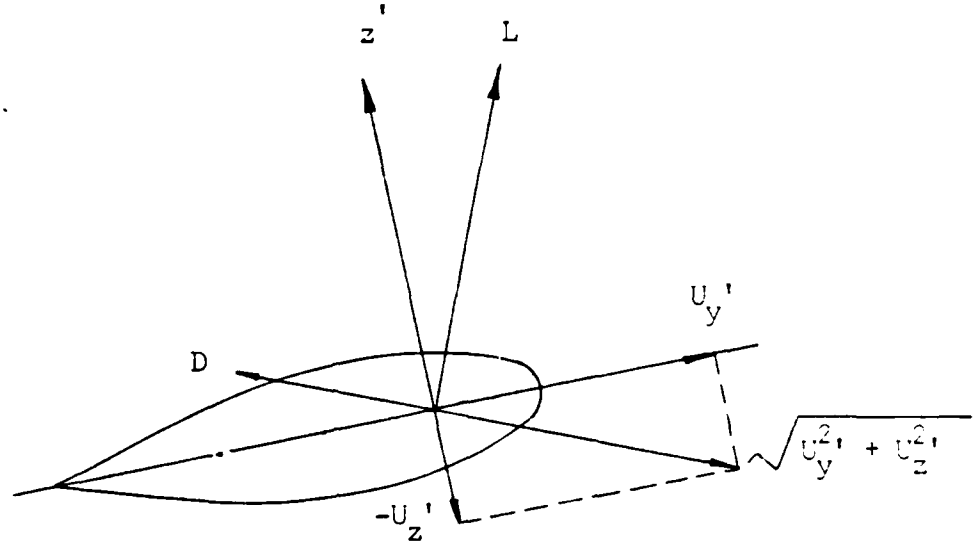

Figure 5 Blade element geometry

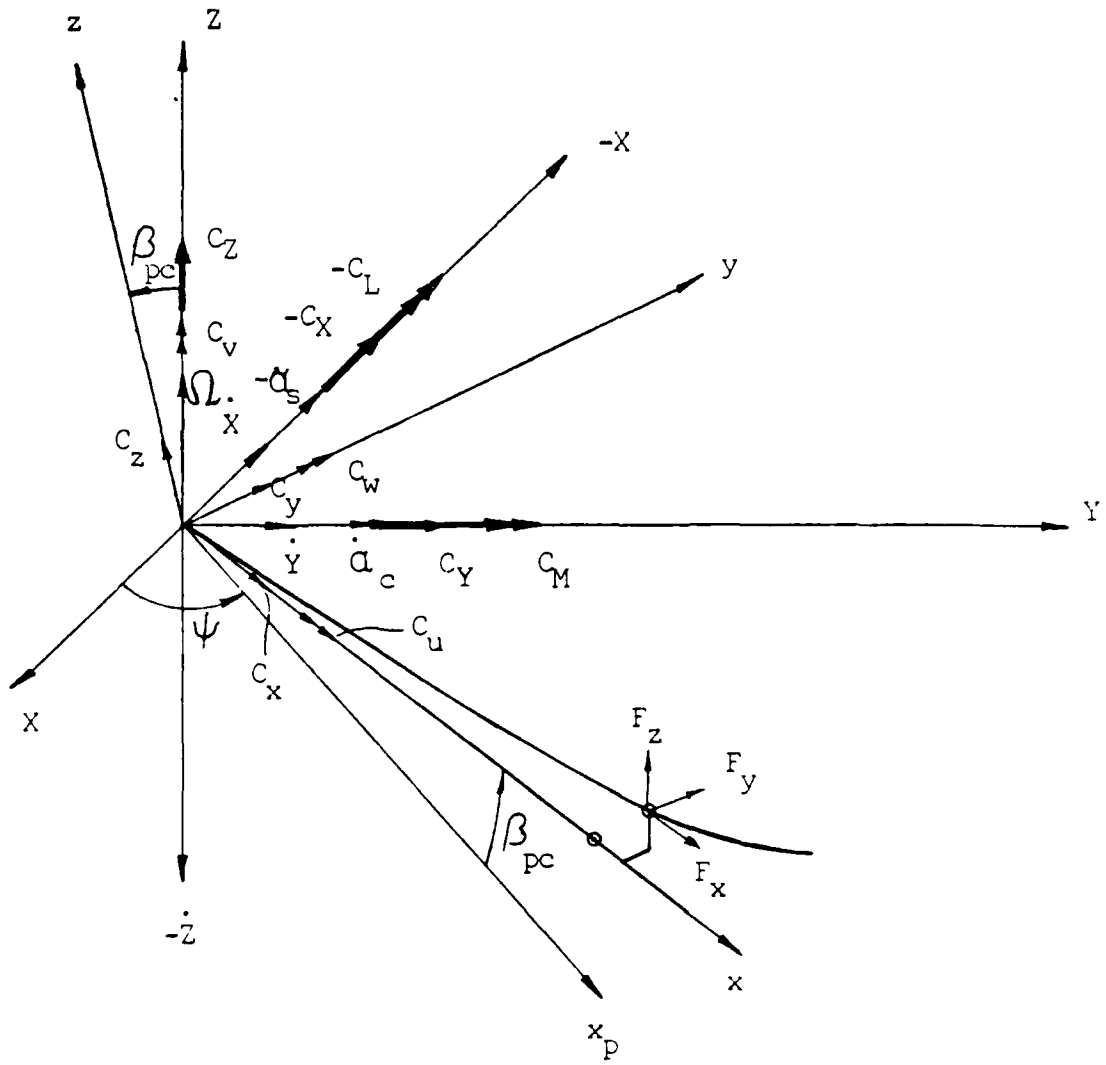

Figure 6 Hub loads

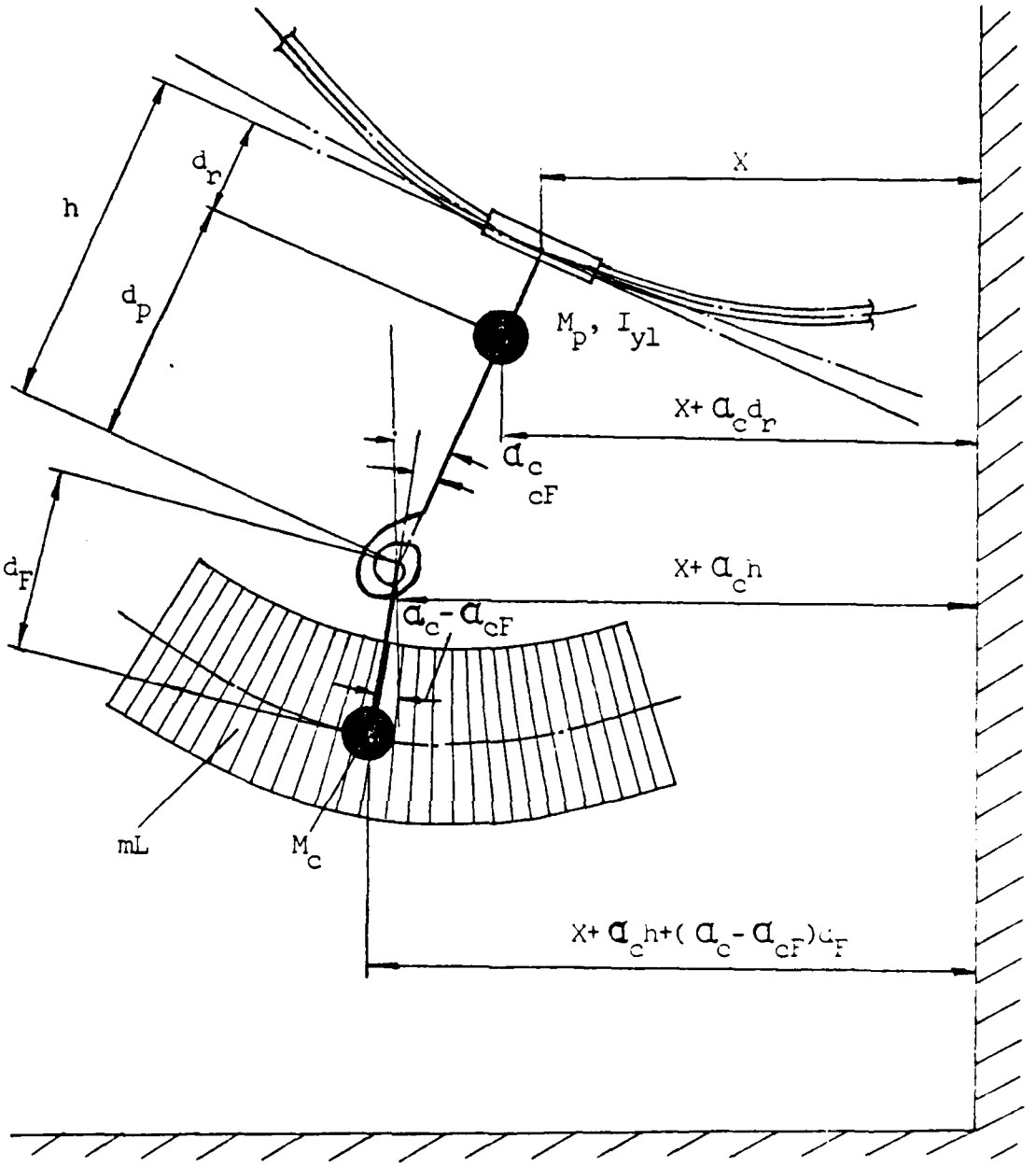

Figure 7 Fuselage model in longitudinal and pitch direction

END

2-87

DTIC